First-principles investigation of gas adsorption on monolayer Rhenium Disulfide (ReS_2)

Thesis submitted to the University of Nottingham for the degree of

Master

Haolun MA, BEng.

20416141

Supervised by

Dr. Hainam Do

Dr. Kien Woh Kow

Table of Contents

Acknowledgements

I want to thank my supervisor, Dr. Hainam Do and Dr. Kien Woh Kow, for their guidance and support. Furthermore, I would like to thank the University of Nottingham Ningbo China, for its supportive academic environment and invaluable academic services - finally, my biggest thanks to my family. I want to express my heartfelt gratitude to my parents and family for their unwavering support throughout my pursuit of a master's degree.

List of Tables

List of Figure

Abbreviations

$n(r)$	Electrical density
ψ_i	Wave function
E_{XC}	Exchange-correlation energy
$E[\{\psi_i\}]$	Total energy of the system
$T[\{\psi_i\}]$	Kinetic energy of the electron
$E_{ne}[\{\psi_i\}]$	Potential energy between Nuclei and electrons
$E_{ee}[\{\psi_i\}]$	Potential energy between pairs of electrons
$E_{nn}[\{\psi_i\}]$	Potential energy between pairs of Nuclei
0-D	Zero-dimensional
1-D	One-dimensional
2-D	Two-dimensional
LOD	Limit of detection
TMDs	Transition metal dichalcogenides
Mxene	2D transition metal carbide and nitride
MoS_2	Molybdenum Disulfide
WS_2	Tungsten disulfide
$MoSe_2$	Molybdenum diselenide
SnS_2	Tin sulfide
HfS_2	Hafnium Disulfide
TaS_2	Tantalum Disulfide
ReS_2	Rhenium disulfide
H	Hexagonal
T	Trigonal
GFN1-xTB	Generalized Force Field 1st Order Tight Binding
CO	Carbon monoxide
CO_2	Carbon dioxide
H_2	Hydrogen
NO_2	Nitrogen dioxide
NO	Nitric oxide
DFT	Density Functional Theory
DOS	Density of states
LDA	Local density approximation
GGA	Generalized gradient approximation
PBE	Perdew-Burke-Ernzerhof functional
VDD	Voronoi Deformation density
CDD	Charge density difference
ELF	Electron localization function
NOCV	Natural Orbitals for Chemical Valence
VB	Valence band
CB	Conduction band
VBM	Valence band maximum
CBM	Conduction band minimum
XC function	Exchange-correlation energy function

Refereed publication

Manuscript in Preparation:

Haolun Ma and Hainam Do, First-principles investigation of small gas molecule adsorpotion on monolayer Rhenium Disulfide (ReS_2), Appl. Surf. Sci. xxx (2023) xxx-xxx

Abstract

The utilisation of 2-D transition metal dichalcogenides (TMDs) holds the potential to improve the efficiency of gas-sensitive electronic devices due to their advantageous semiconductive properties, tunable transport characteristics, and heightened reactivity at active sites. As a member of transition metal dichalcogenides, monolayer Rhenium disulfide (ReS_2) is expected to have the potential as a gas sensitive material. This thesis aims to examine the capability of ReS_2 as a material for adsorption. The adsorption target gases are carbon monoxide (CO), carbon dioxide (CO_2), hydrogen(H_2), nitrogen dioxide (NO_2) and nitrogen dioxide (NO). The methodology employed in this study is rooted in the application of first-principles calculations based on the density functional theory (DFT). In order to determine the most favourable adsorption configuration, we employ a systematic approach by utilizing multiple initial sites and diverse gas configurations as starting points for the optimisation process.

Following the search for the most stable adsorption configuration of gas molecule, the adsorption characteristics of the gas molecules on the energetic favourable configurations are subject to in-depth examination. Our work shows that the adsorption of five gas molecules onto ReS_2 results in a spontaneous process with a release of energy. Meanwhile, the charge transfer direction is from gases to ReS_2, indicating gas molecules and ReS_2 can be considered electron donor-acceptor pair. The outcomes of the analysis of adsorption energy and charge transfer suggest that ReS_2 exhibits low sensitivity towards CO, CO_2, and H_2. Furthermore, the adsorption of these gases does not significantly impact the electronic structure of the ReS_2 monolayer based on the analysis of band structure and density of states. In order to characterise its potential as a gas-sensing material, extra electric field is applied in CO and CO_2 adsorption cases to investigate their adsorption properties on the ReS_2 surface. It has been established that the presence of an electric field has a positive impact on the adsorption capacity of ReS_2 for these two gaseous species. However, in order to achieve a substantial improvement in adsorption, it is imperative to apply a high-intensity electric field.

NO_2 and NO adsorption on ReS_2 show a large and complex interaction between gas molecules and material. ReS_2 has more sensitivity to NO and NO_2 than CO, CO_2 and H_2. The adsorption energy and charge transfer of NO_2-ReS_2 and NO-ReS_2 adsorption systems are -0.512 eV and -0.434 eV, which are far more significant than CO-ReS_2, CO_2-ReS_2 and H_2-ReS_2. The adsorption of nitrogen oxides has led to a significant alteration in the electronic configuration of ReS_2. A significant degree of orbital hybridization between them and ReS_2 is observed. Thus, ReS_2 is an excellent material for NO_2 detection and potential material for NO detection. If ReS_2 is expected to enhance its adsorption properties towards other gases, its sensitivity and selectivity of ReS_2 can be further improved through material modification techniques. This study

can provide a basis for developing ReS_2-based sensors in applications and experiments.

Chapter 1

Introduction

1.1 Motivation

As society progresses, more and more attention has been paid to health, safety, and environmental issues. Gas sensors play a crucial role in addressing these concerns. Since the beginning of the industrial age, gas leakage and emission in industrial production have become growing problems. Gas leakage affects safety and health, as the leaked gas may be toxic, flammable, or explosive.[1] Gas emissions can originate from a variety of sources, including fossil fuel combustion, chemical production, transportation, animal husbandry, and so on.[2] The impact of gas emissions on the environment can have detrimental effects on human health. Problems with smogs and the greenhouse effect are amongst the most familiar gas pollution. The severity of harm caused by gas leaks and emissions has continued to escalate. As a result, the detection of gas is inevitable, and gas sensors have gradually appeared in industrial production and life.

A gas sensor is a technological device that responds to selected specific gases and produces optical or electric signals dependent on their concentrations in real time.[3] It has been approximately a century since the birth of gas sensors used in industry, and the continuous advent of novel applications stimulated further innovations leading to the technological diversity that currently characterizes today's gas sensing industry. Gas sensor technology has thus grown to be indispensable for supporting several aspects of our civil life, yet there remains significant potential for future growth. The development of gas-sensing materials is facilitated by the advent of novel materials, which are capable of interacting with gas molecules and converting them to signals.

Consequently, experiments and computations have been devoted to evaluate the gas-sensitivity properties of various types and configurations of materials to identify superior gas-sensitive materials. Among all alternatives, two-dimensional (2-D) materials have attracted significant attention due to their exceptional atomic-scale electronic and mechanical properties. Most of the reported 2-D materials for gas-sensing exhibit a high limit of detection (LOD) and relatively low sensitivity at room temperature.[4] However, 2-D materials can be formed with different elements and crystal structures. Illustrative examples include graphene, transition metal dichalcogenides (TMDs), 2-D transition metal carbide and nitride (MXene), and monolayer metal oxides, to name a few, which are all typical 2-D materials. Multiple

members of the TMDs family have been employed in the gas sensitive field. Notable is molybdenum Disulfide (MoS_2) and tungsten disulfide (WS_2). Most of the TMDs have the same structures, hexagonal (H) or trigonal (T). For example, MoS_2 and WS_2 crystallize in a 1-H structure, and a single layer of these materials is called a 1-H structure.

On the other hand, Tin sulfide (SnS_2), Hafnium Disulfide (HfS_2), and Tantalum Disulfide (TaS_2) crystallize in a trigonal anti-prismatic structure. N Nevertheless, there is a unique member in the TMD family that distinguishes itself from other members, which have H and T structures. Monolayer Rhenium disulfide (ReS_2) possesses a distorted 1-T structure, which manifests as a disturbed lattice that structure that lacks symmetry. It is neither in the 1-H nor the 1-T phase; the phase transition is primarily driven by the Re atoms.[5] Its particular structure brings new interesting properties for gas-sensing materials and has excellent electronic properties as a gas-sensing material. Hence, ReS_2 presents a tantalizing possibility for more sensitive gas-sensing applications. The principal objective of this thesis is to analyze the gas sensitivity and properties of ReS_2. The target gases are mainly poisonous and harmful small molecule gas: carbon monoxide (CO), carbon dioxide (CO_2), hydrogen (H_2), nitrogen dioxide (NO_2) and nitric oxide (NO).

1.2 Background

1.2.1 Gas sensor

1.2.1.1 History of gas sensor and requirements in the modern society for gas sensitivity

Gas sensing plays a pivotal role in the advancement of detection systems that find wide-ranging applications across diverse domains such as heavy industries, air quality monitoring, and environmental science.[6] The initial purpose of gas sensors was to monitor the concentration of flammable gases in the surroundings to prevent the buildup of concentrations that could potentially reach lower explosive levels, specifically in the case of H_2. Additionally, the gas sensor also serves as a fire detection that detects various gases produced during the combustion of the material.

The genesis of gas sensors can be traced back to the epoch of industrialization, wherein the foremost gas detector of the era featured an oil flame enclosed in a mesh screen to discern firedamp (methane, H_2, and other flammable gases), which was created in 1816.[7] The origins of the gas sensing industry are also from the need to detect flammable gases. Dr.Oliver Johnson created the hot wire catalytic platinum filament in around 1926 to detect combustible vapours in the petrochemical industry.[8] Presently, the detection of the lower explosive limit (LEL) of flammable gases and the vapour phase of flammable liquids has acquired paramount significance, given the potential hazards associated with their inadvertent discharge. Consequently, it is

essential to possess reliable and exact measuring instruments to ensure public safety.[9]

Health and safety legislation has also imposed an additional requirement for the implementation of gas sensors, further expanding the scope of their use in ensuring public welfare.[1] As industrial production advances, the detection and alarm of toxic gas molecules become critical in specific industries where human exposure to such gases is a possibility. For instance, ammonia, a commonly produced gas in diverse industrial processes, is recognized for its irritant and corrosive properties. Occupational Safety and Health Administration, which is part of the U.S. Department of labour, has reported that the highest concentration of ammonia that humans can contact is 50 ppm and the permissible ammonia gas exposure limit in the working place is 25 ppm.[10] ammonia above 50 ppm, even also at low concentrations, can cause severe irritation to the throat, nose, eyes, skin, and respiratory.[11] Moreover, various toxic and harmful gases have been produced during industrial production, with the increase in industrialization, such as chlorine, hydrogen sulfide, nitrous oxide. Consequently, it is imperative to produce gas sensors of high calibre to safeguard human health. In the last few decades, several types of gas sensors have been developed and utilized in the domain of occupational health and safety.[12]

Following the establishment of health and safety standards, gas detection has also emerged as a vital component of environmental science, encompassing minor molecular gases and diverse volatile organic compounds associated with air pollution[13]. More and more harmful and toxic gases are discharged into the environment due to uncontrolled industrialization and fossil fuel in the recent past. These anthropogenic toxic pollutants are released into the atmosphere, destroying the environment and harm to people. For example, burning fossil fuels will emit carbon dioxide (CO_2), nitrogen oxides, sulfur oxides, and carbon monoxide (CO).[14-16] CO_2 emission occupies 77% of Greenhouse gases emissions, and thus it has become the primary reason for significant anthropogenic climate change.[14, 17] Nitrogen oxides and sulfur oxides cause the formation of photochemical smog and acid rain.[16, 18] CO is a toxic gas that is both odour-less and colour-less and a high affinity for haemoglobin, binding to it approximately 200 times more strongly than oxygen, which results in a significant reduction in the capacity of haemoglobin to transport oxygen, leading to tissue hypoxia.[19] Of course, in addition to minor molecular gases, Volatile organic compounds are a significant source of air pollution and public health risks. Volatile organic compounds are a major class of air pollutants that have been linked to the formation of photochemical smog, as well as potential health risks such as carcinogenesis, teratogenesis, and mutagenesis.[16] Furthermore, they can come from almost every daily activity of human beings, and a large number of industries and processes that usually emit a high level of volatile organic compounds have been born since the industrial revolution.[20] So, environment science has once again broadened the application field of gas sensors, such as air pollution monitoring in environments.[21]

In recent decades, the emergence of new applications and technologies has

expedited the research and development of gas sensing with greater sensitivity and convenience.[9] LOD, sensitivity, selectivity, recovery time and response time are all the general parameters that should be considered in research and experiment, and certain factors need to be considered in particular applications. Meanwhile, special gas sensing needs from modern society and emerging industries need to be met, such as wearable gas sensors, energy harvesting, and self-powered gas sensors.[22] As a whole, sensors have plenty of room for further growth in the future.

Gas sensors can utilize electronic components such as resistors, diodes (Schottky or p-n diodes), FETs, and capacitors. However, as chemical sensors, gas sensors are composed of a sensing material (active layer) and transducing element.[23, 24] Target gas molecules interact with sensing materials which modulate overall conductivity (resistivity) via charge transfer interactions between constituent atoms of a gas molecule and the sensor material, so physical change is transformed into electronic signals, such as a change in the resistance, frequency, current, or voltage.[24, 25] Sensing materials are responsible for interacting with gas molecules, so it has a massive impact on gas detection results. Thus, the extremely low detection limit for hazardous gases is expected to be lower with the development of research on the gas-sensing properties of sensor materials. New gas-sensing materials can accelerate the development of gas sensors. To develop gas-sensing materials, some specific criteria of effective gas sensor material should be met. One crucial criterion is having a large surface area, which increases the number of reactive sites available for gas molecules. It is also vital that these materials possess appropriate semiconductor electronic properties and ample reactive sites to ensure high sensitivity and selectivity for target gases. By optimising these characteristics, gas-sensing materials can enhance gas-sensing technology.[25]

1.2.1.2 Gas sensor materials

Researchers have extensively investigated diverse materials as potential candidates for gas-sensing applications, including semiconductors, optical fibres, conjugated polymers, low dimensional nanomaterials, and so on.[24, 26, 27] Most materials have their advantages and disadvantages. For example, semiconductor metal oxides have the advantage of a simple preparation process, low cost, and high integration, but their operating temperature should be high, and selectivity is low; conjugated polymers are unstable and have poor recovery.[28] Among all materials for gas-sensing applications, 2-D materials are attractive due to high surface-to-volume ratio, tunable electronic properties, and variety of 2-D materials with different compositions and structures.[29]

Although many gas sensors based on 2-D materials have been realized, gas sensor researchers and developers expect a lower shallow detection limit for hazardous gases. Therefore, research on the sensitivity of a 2-D material to a gas is essential. Both experiments and theoretical calculations have been employed to push the frontier in this area.

1.2.2 Two-dimensional materials and TMDs materials

1.2.2.1 Application of low-dimensional materials for gas sensing

Low-dimensional materials are defined by one or more characteristic lengths of materials confined to the atomic scale, high dispersibility or ductility, and outstanding electrical properties. Low-dimensional materials, including zero-dimensional (0-D), one-dimensional (1-D), and two-dimensional structures, exhibit unique characteristics of gas sensing. Three different low-dimensional materials have their advantages and disadvantages. 0-D nanomaterials have the most active sites and surface-to-volume ratios, but they will not be directly used as electronic components. Coarsening and agglomeration of 0-D tiny particles during the gas sensor fabrication will reduce its sensitivity or increase detection limit. 0-D materials are mainly used for deposition on 1-D or 2-D materials to enhance sensitivity.[30-32] The sensor response to the same gas on 1-D nanowires gas sensor was higher than those of 2-D-based devices, but the sensor based on 2-D nanostructures has a much higher LOD. Because the sensor response varies with dimensionality and the average size of the nanostructures composing the active material, a larger cross-sectional area permits a more stable base current.[33]

1.2.2.2 2-D materials

The discovery of the first 2-D material, the graphene monolayer, has increased interest in exploring other 2-D materials because of their unique structural and physicochemical properties. In recent years, the investigation of 2-D nanomaterials has become an increasingly important area of study, which have significant impacts on a wide range of applications in various fields.[34-36] So far, 2-D nanomaterials have been used in various applications, including biomedicine, optoelectronics, electronics, sensing, energy conversion and storage.[37-41] In particular, due to the large surface area, unique and often superior properties, which facilitates surface reactions, 2-D nanomaterials have significant advantages in the field of gas sensing applications

Graphene, as the first 2-D material manufactured, is the beginning of a detailed understanding of 2-D materials. It is a 2-D layered material composed of a single layer of graphite, where carbon atoms are arranged in a crystalline lattice with sp2 hybridization in the shape of a honeycomb.[42, 43] It was always believed that planar graphene itself did not exist in a free state until Geim and Novoselov discovered independently graphene in 2004. At the same time, the existence of graphene indicated that strictly 2-D materials could exist at finite temperatures.[44] Graphene concerns researchers in various fields due to its outstanding conductivity, high carrier mobility (2000 $cm^2V^{-1}s^{-1}$) at room temperature, good thermal conductivity, high surface-area-to-volume ratio, mechanical strength, and stability.[45] Since Novoselov's

experiment on the adsorption of gas molecules on graphene.[41] The gas sensitive detection of graphene and its derivatives has never stopped. The graphene-based gas sensor is just the beginning. Graphene oxide and reduced graphene oxide are used in the gas sensing field. However, the absence of an electronic bandgap in graphene limits its development, and thus researchers have had to continue developing new 2-D materials.[46, 47] Subsequently, Si, Ge, and Sn, which are elements located underneath carbon that belong to central group IV, can also form the resembling graphene monolayer structure with H lattices called silicene, germanene, and stanine.[48-50] Moreover, the elements of the group adjacent to the carbon element are also successively manufactured into 2-D materials, and their gas sensing properties are predicted and tested, such as phosphorene, arsenene, antimonene, borophene, tellurene and bismuthine[51-55]. These are 2-D materials composed of single elements: black phosphorus, Arsenic, Antimony, Boron, Tellurium, and bismuth.

The 2-D materials mentioned in the previous paragraph are all single-element graphene-like 2-D materials. The utilisation of graphene, germanene, and other single-element analogues of graphene for Field Effect Transistor (FET) sensors has been in rapid development.[56] Despite their success, these mono-element 2-D materials still have much potential for further improvement. For example, the zero band gap of germanene and graphene has remarkably high carrier mobility but makes it difficult to turn off the transistors.[57] Thus, 2-D materials containing various elements have been characterized, and their appearance can enrich the functions and applications of 2-D materials.

The family of 2-D materials includes a vast array of members, which have been synthesized experimentally or predicted through theoretical studies. As a result, there is a rich diversity of multi-element 2-D materials available. 2-D transition-metal carbides/nitrides (collectively denoted as MXenes), 2-D Transition metal dichalcogenides (TMDs), and monolayer metal oxides (MO) are all conspicuous non-single-element in 2-D materials.

MXenes, a family of transition metal carbides and/or nitrides, is 2-D material that naturally resembles graphene. First reported by the Barsoum's group in 2002 has been among the most recent and notable 2-D materials.[58-60] Ti_3C_2TX is the first MXenes 2-D material successfully delaminated from Ti_3AlC_2 in 2011. MXenes are obtained from the MAX phase($M_{n+1}AX_n$, n=1 to 3) by selective etching and exfoliation process, where M is an early transition metal, A is an A-group (mostly IIIA and IVA, or groups 13 and 14) element and X is either carbon or nitrogen.[23, 61] The 'MXene' is also from 'MXA', which emphasizes the loss of the A element and the nature of 2-D materials resembling graphene by 'ene'.[34]

2-D MO as a nanostructured oxide, is exfoliated from its layered parent materials, which is the simplest manufacturing method. The mechanical exfoliation method of MO differs from the other two manufacturing methods, TMDs and MXenes mainly depend on lattice growth.[62-64] The 'M' in 2-D MO could be: = Cu, Co, Fe, Sn, Zn, Ni. TMDs are mentioned last and have become a subject of extensive research due to

their exceptional properties, including their strong spin-orbit coupling, direct bandgap structure, unique atomic-scale thickness, and favourable electronic and mechanical characteristics.[29, 55, 57, 61, 65] Gas sensing is a crucial area of exploration in these material studies, as researchers focus on understanding the adsorption properties and interactions of 2-D materials with gases.

1.2.2.3 TMDs

The material chosen for investigation in this thesis is ReS_2, which belongs to a class of 2-D materials not previously mentioned, known as TMDs that has been mentioned in the previous text. TMDs are composed of MX_2 compounds. M could be any transition metal from an IVB-VIA metal element, which includes insulators or semiconductors, to metallic or semi-metallic (including Ti, V, Nb, Ta, W, Zr, Re, and so on), and X is a chalcogen, specifically Se, S, or Te.[55, 61]

All the considered TMDs members were synthetic, except for MoS_2, which was a natural TMD monolayer. They could be mechanical and chemical exfoliation of its layered bulk counterparts, as well as through chemical vapour deposition.[65] Due to high scalability and morphological control, chemical vapour deposition has become the most valued and widely studied method. In the chemical vapour deposition process, the metal-containing precursors that are being vaporized react with the solid phase sulfur element, and 2-D TMDs grow on the substrate downstream.[66] Furthermore, the members of the TMDs family form various kinds of lattice structures with different physical properties.

From the orientation point of view, most of the TMDs monolayers exhibit a 1-H or 1-T structure with a single-layer sandwich structure (X–M–X) that is a transition metal atomic layer between two chalcogen atomic layers stacked together through comparatively feeble van der Waals forces, which might be considered as a graphene-like structure material.[55, 67] Atomic thin 2-D TMDs nanostructures are a graphene-like layered semiconductive analogue of graphene with more optimistic application potential

Zero band gap leads to graphene having remarkably high carrier mobility but makes it difficult to turn off the transistors. On the contrary, many members in the TMDs family have a wide range of bandgap and are better suited for their use as electronic devices in sensors.[65] However, only some TMDs materials are suitable semiconductor materials with an excellent direct band gap for electronic components. Some of the TMDs exhibit metallic properties that have a similar problem to graphene, that zero gap or narrow gap. The bandgaps of them are shown in **Table 1.1**. TMDs with narrow or zero bandgap are the same as metal; others show semiconductor properties.

Table 1.1 Band gap of TMDs family members

Materials	Gap (eV)	Materials	Gap (eV)
WS_2	~1.8	VS_2	~0- 0.3
WSe_2	~1.6	VSe_2	0
WTe_2	0	VTe_2	~0
HfS_2	~1.2 -1.3	ReS_2	~1.4
$HfSe_2$	~0.6	$ReSe_2$	~1.3
$HfTe_2$	~0.21	TiS_2	~0
ZrS_2	~1.12	$TiSe_2$	~0
$ZrSe_2$	~0.54	$TiTe_2$	~0
$ZrTe_2$	~0.075	NbS_2	~0
MoS_2	~1.8	$NbSe_2$	~0
$MoSe_2$	~1.44	$NbTe_2$	~0
$MoTe_2$	~1.1	TaS_2	~0.213
CrS_2	~0.93	$TaSe_2$	~0.153
$CrSe_2$	~0.75	$TaTe_2$	~0
$CrTe_2$	~0.53	$TcSe_2$	1.14
TcS_2	1.28		

1.2.2.4 TMDs materials for gas sensor

2-D TMDs materials, which possess non-zero band gap semiconductor properties, have opened new avenues for gas-sensing materials. Compared to graphene, 2-D TMDs exhibit superior gas sensitive electronic device characteristics, including semiconductive properties, tunable transport characteristics, and a greater number of reactive sites.[68] The adsorption properties experiments and calculations on TMDs are starting from MoS_2. Common small gases, such as NO_2, NO, CO_2 and SO_2 were firstly chosen for adsorption studies on the pristine monolayer MoS_2 using first-principle calculations.[69, 70] According to the calculated data, the gas sensing experiments of MoS_2 is carried out. For example, the MoS_2 shows a low LOD of NO_2

(120 ppb).[71]

Since TMDs came into the spotlight a long time, MoS_2 accounts for most scientific efforts in manufacturing and applications.[25] Then, the gas sensitive properties of 2-D TMDs materials, including $MoSe_2$, WS_2, and $HfSe_2$, have been extensively studied by experimental and theoretical calculations.[65, 72, 73] The TMDs materials mentioned above are relatively mature gas-sensing materials. Compared to them, a TMDs material with a special structure and excellent properties of electronic called ReS_2 only has rare gas sensing research. However, it shows extremely sensitive adsorption characteristics to some minor molecular gases.

1.2.3 Rhenium disulfide (ReS_2) in TMDs family

ReS_2 is expected to be used in gas sensing due to new exciting properties of gas-sensitive materials caused by deformity structure. New properties may bring properties of higher sensitivity and special applications in the gas sensing field. Meanwhile, ReS_2 has excellent properties as an electronic component. However, it may be constrained by the cost or difficulty of manufacturing. In addition, there are only a few experiments and computational studies of ReS_2 adsorption. Attention has not been paid to the research of ReS_2 monolayer in the field of gas sensing. Thus, this study hopes to open the door for the characterization of small gas molecules and ReS_2.

1.2.3.1 ReS_2 in TMDs family

2-D TMDs have been extensively researched and applied in various fields. Among them, group-VI members such as tungsten and molybdenum have gained intensive attention, and materials such as MoS_2, $MoSe_2$, WS_2, and WSe_2 have been extensively studied for several years. However, some 2-D materials with peculiar structures are challenging to mass-produce due to technical problems and a lack of experiments and research.

ReS_2 is a member of the TMDs family, specifically, a ‘group 7’ member, composed of Rhenium and Sulfur elements. Its layered structure consists of two layers of sulfur atoms enclosing a layer of rhenium atoms in a sandwich-like arrangement. The Re is a d-block transition metal with d^n configuration (n = 0–8), and stable compounds form with S element only with d^3 configuration.[74] The unit cell of ReS_2 includes four Re and eight S atoms due to metal-metal bonding, which is different from other TMDs family members.

1.2.3.2 ReS_2 structure and lattice constant properties

2-D ReS_2, like other TMDs materials, comprises three atomic layers (Re-S-Re) held together by weak van der Waals (vdW) forces to form bulk crystals. However, unlike most TMDs, 2-D ReS_2 does not possess a 1-H or 1-T structure. Instead, its

monolayer structure crystallizes in the distorted-1T phase and exhibits a distorted 1-T phase, denoted as 1-T'.[75-77] The unique 1-T' structure sources are Re atoms. Re atom has seven valence electrons; when Re atoms exist in a 1-T or 1-H structure, every Re atoms have an extra electron. The extra electron contributes to the formation of Re-Re bonds, so total energy reduces, and Eigenvalues of the acoustic phonons become real and distorted-1T structure format. Finally, a unit cell is derived from hexagonal symmetry towards a distorted 1T structure.[5, 74]

The later lattice constant of ReS_2 provided by the experiment is a = 0.6352 nm, b = 0.6446 nm, c = 1.2779 nm.[78] Density functional theory (DFT) calculation also can support the lattice constant of monolayer ReS_2 which is s a = 6.42 Å and b = 6.52 Å.[5] Of course, the DFT calculation about ReS_2 is not practical, but it should be close to experimental data.

1.2.3.3 ReS_2 special properties from 1-T' structure

ReS_2 exhibits extraordinary properties due to its unique distorted 1T structure, which distinguishes it from other more common TMDs that have been widely studied. The Re atoms in ReS_2 form a diamond-shaped cluster, which in turn interlinks to form diamond-shaped chains along the van der Waals plane, leading to in-plane anisotropy in the material.[75, 77] ReS_2 has the highest anisotropic ratio of 3.1 (along the two principal axes) in the TMDs family. High anisotropic brings one potential application to enhanced error tolerance to gas sensors when detecting target gas, via measurement of horizontal and vertical directions electric currents.[79, 80]

Among all TMDs, ReS_2 is unique and receives great attention due to its nearly layer-independent vibrational, thermal, optoelectronic and physicochemical properties, which are different from other TMDs.[5] The layer-independent property is due to weak interlayer coupling caused by ReS_2 distorted structure.[5, 81, 82] Take the band gap as an example, one of the prominent properties of TMDs is that their band gaps are modulated by thickness, they undergo a crossover from indirect band gap in the bulk to direct bandgap in a monolayer and only monolayer TMDs exhibit direct bandgap.[83] Nevertheless, on the contrary, ReS_2 has a most significant feature that remains a direct bandgap semiconductor from bulk to monolayer (bandgap =1.35 eV of bulk and 1.43 eV of monolayer).[5] In other words, ReS_2 have nearly identical band structures under any thickness.[5, 83, 84] In particular, ReS_2 bulk acts as if it is electronically and vibrationally monolayers.[5, 61] Bulk ReS_2 could be an ideal platform to study 2-D ReS_2 lattice physics, which does not need to mass manufacture a single layer.[5]

Finally, ReS_2 has a 1T distorted octahedral structure with triclinic symmetry.[83, 85] Peierls distortion in the 1T structure of ReS_2 leads bulk to behave as electronic and vibrational decoupling, which causes anisotropy in optical and electrical properties.[5, 75] These various phases and novel electronic properties were elaborated by Tongay's Group.[5]

The advantages of 2-D ReS_2 are summarised: 1) It exhibits a wide range of special

physicochemical properties that like other 2-D materials, meanwhile 2-D and three-dimensional ReS_2 show no different properties; 2) The ReS_2's band gap in Table1 shows close to band gaps of $MoSe_2$, MoS_2, and WS_2, which mean it could be a good choice for electronic components, and an unchangeable band gap is also suitable for device design; 3) Extremely high anisotropic may bring wonders in future gas sensing applications

1.2.3.4 ReS_2 as the basic properties of electronic components

In addition to these special properties from the deformed structure, ReS_2's outstanding physical properties have attracted attention. ReS_2-based field-effect transistor possesses a high room-temperature current on/off ratio (~10^7) and high carrier mobility (79$cm^2V^{-1}S^{-1}$).[79, 86] A high on/off ratio provides better stability and anti-interference ability; carrier mobility determines the suitability of materials for applications in electronic devices, and higher current charge capacitances determined by high carrier mobility can result in higher frequency response.[87] So, ReS_2 can be a suitable material for electronic devices, including gas sensors. ReS_2 also shows strong interaction with nonmetal adatoms (H, N, P, O, S, F), which increases interests in its potential in the field of gas detection.[85] In summary, the special properties of distorted structure and other properties of ReS_2 with low symmetry can be exploited for novel applications in future electronics.[79]

1.2.3.5 Experiment and Calculation of ReS_2 in Gas Sensing Field

ReS_2 has already demonstrated promising applications in optical sensitivity, energy storage, solid-state electronics, and energy harvesting.[76] However, there is currently a lack of experimental and theoretical research on the gas sensing properties of ReS_2. This may be attributed to the challenges associated with the manufacturing process of ReS_2, which can be both difficult and expensive. Most TMDs materials with semiconductor properties have been tested or simulated for gas sensitivity, but ReS_2 has rarely been studied in the field of gas sensitivity. Only a few experiments and calculations on small molecule gas adsorption and volatile organic compounds adsorptions have been reported.[4, 88] These two studies both incorporate light conditions. ReS_2 in the adsorption experiment of nitrogen dioxide shows ultrahigh sensitivity (response of 9.07 at 500 ppb) and a low LOD (50 ppb). At the same time, it also shows a brief total response time (55s) and recovery time (180s). The total response and recovery time of ReS_2 transistor-based gas sensors toward ppb level NO_2 is one of the top three shortest in the TMDs family. Under visible light illumination, ReS_2 also has a reversible NO_2 response, which is superior to MoS_2. In the recent gas adsorption calculation, ReS_2 is also verified to have highly selective NO_2 gas sensing.[89] The excellent performance of ReS_2 for NO_2 and H_2O adsorption makes it a promising candidate for ultrasensitive room-temperature gas sensors. It is

noticed in its adsorption performance for other small molecule gases.[4, 90, 91]

Nevertheless, compared with those who belong to the TMDs family - MoS_2, WS_2, $MoSe_2$,[65, 72, 73, 92] ReS_2 is still the least studied in gas sensing. The reason may be the difficulty and cost of ReS_2 manufacturing while a more convenient manufacturing method of ReS_2 is gradually developed.[93] However, ReS_2's special structure from Re-Re metal and properties make us interested in its gas sensing properties. First principles calculation with DFT method for adsorption properties of ReS_2 before going for expensive experimentation could provide valuable insights. Theoretical calculation of 2-D ReS_2 can enable the study of underlying sensing mechanisms and the analysis of the sensor performance.[61, 94] The data can also provide a basis for developing ReS_2-based sensors in applications and experiments. In order to explore the possibility of 2-D ReS_2 as a gas-sensing material, the common poisonous and harmful small molecule gas (CO, CO_2, H_2, NO_2 and NO) will be the target gas.

1.3 Thesis outline

This thesis is organized into the following six chapters:

Chapter 1 introduces the requirements of gas sensitivity, as well as the possibility and properties of ReS_2. In addition, the goal of this paper has been determined, which presents a theoretical picture of the nature of homogeneous gas adsorptions on ReS_2.

In chapter 2, the main content is to describe the First-principles calculation based on DFT and its application in gas sensing. As a powerful tool in materials sciences, first principles calculation approach is compelling for predicting potential applications of materials and accordingly provides useful information for guiding experiments. The adsorption type and properties we need from the calculation are explained in detail in this chapter. Finally, a brief introduction to the computing software that used in this study is included.

Chapters 3-5 recorded the optimisation results of the ReS_2 monolayer and the adsorption results of 5 gas molecules. First, the unit cell of ReS_2 was optimised and optimised data is summarised in chapter 3. Subsequently, configuration optimisations of optimised materials and gas molecules are presented in chapters 4 and 5.

Chapter 6 provides a concise summary of the prior computational findings and potential applications of ReS_2. Furthermore, it discusses potential avenues for further research, specifically in the area of ReS_2 gas sensing properties. The chapter ends by outlining possible extensions for ReS_2 research, thereby highlighting its potential as a versatile and high-performance 2-D material.

Chapter 2

Simulation Methods

2.1 Synopsis

Chapter 2 presents the methodology employed in this thesis, starting with a discussion of first principles calculations. The primary focus of this chapter is to introduce density functional theory (DFT) as a tool for first principles calculations, which is subsequently utilised in other chapters. DFT has broad applicability in various disciplines, including physics, chemistry, materials science, and other branches of engineering.[95] The chapter provides a detailed explanation of the theoretical basis of DFT and its practical implementation, including various approximations and numerical techniques that are commonly used in DFT calculations. In addition, the settings used for the calculations and the adsorption properties studied in the calculation are also listed and explained. The adsorption properties enable the screening of adsorption configurations, elucidation of the gas-ReS_2 interaction, and determination of the electronic structure of the system.

2.2 First principles calculation and use for nanomaterials

In modern scientific research, "computation" plays an increasingly important role. Theoretical calculations offer a clear advantage over traditional experimental methods by saving time and effort, which translates to cost savings. The traditional 2-D material adsorption experiment is expensive, and it is difficult to manipulate the small-molecule adsorptions experimentally. Computational approaches can provide valuable insights into the fundamental interactions between gas molecules and sensing materials, including gas molecules' adsorption energies and diffusion pathways on the material surface. Thus, theoretical calculations of 2-D sensing materials offer a promising pathway for developing gas sensing materials, enabling the study of underlying sensing mechanisms and the analysis of sensor performance before engaging in expensive experimentation.[61, 94, 96] Theoretical calculations can also play a vital role in the design of new material structures and their functionalities.

As an essential tool in computational chemistry/physics and materials science, the first principles calculation method is compelling for predicting materials' potential applications and provides valuable information for guiding experiments. First-

principles calculations are a unique and elegant approach to studying materials that require no empirical parameters beyond fundamental physical constants. First-principles calculations begin by directly solving the mathematical equations that describe the physical laws governing a given system. These methods are particularly well-suited for highly accurate analyses of atomic or electronic-scale problems, they can account for complex interactions and phenomena that would be difficult or impossible to capture using traditional experimental methods alone.[97]

First-principles calculations have the potential to significantly impact electronic nanomaterials and device research by providing accurate insights into the electron configuration of a molecule or solid. Electronic structure calculations, which determine most of the physical properties of matter through chemical bonding, are a crucial aspect of this approach. DFT, Projection operator methods and Perturbation theory are all first-principles theoretical tools of statistical mechanics, forming the foundation of the modern understanding of thermodynamic and transport properties in systems consisting of three or more quantum or classical particles, whether real or virtual.[98-101] Among them, the first-principles calculations that basis on the DFT have been implemented to compute material properties since the early 1980s.[102]

2.3 Density Functional Theory (DFT)

The adsorption of 2-D materials falls under surface science, and DFT-based first principles calculations have proven to be effective partners in numerous successful projects.[100] Geometry and electronic structure of surfaces play a critical role in material science, and DFT can provide insights into the underlying physics of this phenomenon.[95] DFT is a powerful and revolutionary computational tool for first principles calculations developed in the last century. It has the ability to calculate a range of micro and macro properties, including the DOS, band structure, compressibility, phonon spectra, vibrational frequencies, and binding energy.

DFT has been proposed as a means to mitigate the challenges posed by electron interaction in many-body electron structures. The impact of electron interaction is widely recognized as one of the most complex issues in any electronic structure calculation, especially interacting with many-body systems.[97] The Schrödinger equation can be applied to describe the behaviour of an entire many-body electron system. However, its exponential growth in dimensionality with the number of particles creates a deceptively simple linear eigenvalue problem that is computationally demanding and can only be exactly solved for very small systems.[101] Meanwhile, the wave function cannot be physically observed.

First-principles electronic structure calculations are usually performed within the single electron picture using either quantum chemistry (i.e. post Hartree-Fock) methods or, as an alternative to wave function-based methods, DFT associated with the Kohn-Sham equations.[101]

The quantum chemistry method described so far for calculating electronic structure

depends on knowledge of a wave function. However, all wave function basic methods have the same difficulties as Schrödinger equation method. They depend on the 4N coordinates of every electron in the system that an electron has three spatial coordinates and one spin coordinate, which gives the N -electron wave function a vast dimensional complexity. Hartree-Fock could be used in a system with very few atoms, and the calculation cost increases exponentially with the increase of atoms.

Compared to the wave function approaches, DFT can deal directly with the one-electron density and circumvent consideration of the many-electron wavefunction.[103] In other words, DFT changes the simulation's basis from wave function to electron density. Because, in principle, any observable (equilibrium) quantity of a many-body system other data can be derived from the information of ground-state density. While DFT still falls short of the systematic accuracy achievable by traditional quantum chemistry techniques, it is a highly effective method for electronic structure calculations in atomic or molecular systems of intermediate to large scales.[101, 103, 104] First, the calculation of electrical density is the most important in the DFT. As an observable, electrical density also could be calculated by wave function:

$$n(r) = 2\sum_i \psi_i^*(r)\psi_i(r) \tag{2.1}$$

In the above equation, $n(r)$ is the electrical density, ψ_i is the wave function, ψ_i^* is the complex conjugate of ψ_i , and r is a set of coordinates.

It has been mentioned above that DFT is related to Kohn sham equations. Almost all DFT are performed within Kohn–Sham scheme. At the heart of the entire field of DFT lie two foundational mathematical theorems established by Hohenberg and Kohn, and a set of equations derived by Kohn and Sham.[95] The theorems are each:

1) *The ground-state energy from Schrödinger's equation is a unique function of the electron density.*

2) *The electron density that minimizes the energy of the overall function is the true electron density corresponding to the complete solution of the Schrödinger equation.*

The first theorem proves an electron density equation could solve Schrödinger equation, but it does not ensure what the function is. The second theorem establishes the notion of a true electron density corresponding to the complete solution of the Schrödinger equation. If the functional form is known, the relevant electron density could be found by changing the electrical density until the energy is minimized. It becomes a typical variational principle with approximate forms of the functional. This function that connects wave functions and electrons density is Kohn –Sham equation:

$$\left[\frac{h^2}{2m}\nabla^2 + V(r) + V_H(r) + V_{XC}(r)\right]\psi_i(r) = \varepsilon_i\psi_i(r) \tag{2.2}$$

This equation is from the energy function which follows the second theorem:

$$E[\{\psi_i\}] = T[\{\psi_i\}] + E_{ne}[\{\psi_i\}] + E_{ee}[\{\psi_i\}] + E_{nn}[\{\psi_i\}] \quad (2.3)$$

$E[\{\psi_i\}]$: Total energy of the system
$T[\{\psi_i\}]$: Kinetic energy of the electron
$E_{ne}[\{\psi_i\}]$: Potential energy between Nuclei and electrons
$E_{ee}[\{\psi_i\}]$: Potential energy between pairs of electrons
$E_{nn}[\{\psi_i\}]$: Potential energy between pairs of Nuclei

This equation is to calculate the total energy of the system, Kohn and Sham introduce orbitals into the equation to increase the accuracy of kinetic energy calculation $T_{KS}[\{\psi_i\}]$. It is an ingenious indirect approach, $T_{KS}[\{\psi_i\}]$ is close to actual kinetic energy $T[\{\psi_i\}]$ but not equal, so the difference between them also needs attention.

Meanwhile, the $E_{ee}[\{\psi_i\}]$ could be divided into two parts: classical repulsion-Coulomb interaction between electrons $J_{ee}[\{\psi_i\}]$, and he nonclassical term - quantum mechanical effects between electrons. Now, the quantum mechanical effects between electrons and the difference between actual kinetic energy $T[\{\psi_i\}]$ and Kohn-Sham (KS) method kinetic energy $T_{KS}[\{\psi_i\}]$ can be combined into $E_{XC}[\{\psi_i\}]$(Exchange-correction Energy). The $E_{XC}[\{\psi_i\}]$ can be expressed as:

$$E_{XC}[\{\psi_i\}] = T[\{\psi_i\}] - T_{KS}[\{\psi_i\}] + \text{quantum mechanical effects} \quad (2.4)$$

So, the equation can be shown as:

$$E[\{\psi_i\}] = T_{KS}[\{\psi_i\}] + E_{ne}[\{\psi_i\}] + J_{ee}[\{\psi_i\}] + E_{XC}[\{\psi_i\}] + E_{nn}[\{\psi_i\}] \quad (2.5)$$

Moreover, the equation can be expended:

$$E[\{\psi_i\}] = \frac{h^2}{m}\sum_i \int \psi_i^* \nabla^2 \psi_i d^3r + \int V(r)n(r)d^3r + \frac{e^2}{2}\int\int \frac{n(r)n(r')}{|r\ r'|} d^3r\, d^3r' + E_{XC}[\{\psi_i\}] + E_{nn}[\{\psi_i\}] \quad (2.6)$$

The above equation can be further simplified to show the relationship between electron density and wave function, and the final function is Kohn –Sham equation (2.7):

$$\varepsilon_i \psi_i(r) = \left[\frac{h^2}{2m}\nabla^2 + V(r) + V_H(r) + V_{XC}(r)\right]\psi_i(r) \quad (2.7)$$

In this equation, only $V_{XC}(r)$ is not ensured and is hard to be calculated because of $E_{XC}[\{\psi_i\}]$, which includes difference and quantum mechanical effects. $V_{XC}(r)$ is included in another formula $E_{XC}[\{\psi_i\}]$(Exchange-correction Energy):

$$V_{XC}(r) = \frac{\delta E_{XC}\,[n(r)]}{\delta n(r)} \tag{2.8}$$

Now, the electron density can be computed iteratively and applied to Chemical calculations and Physical calculations follow the steps (**Figure 2.1**):

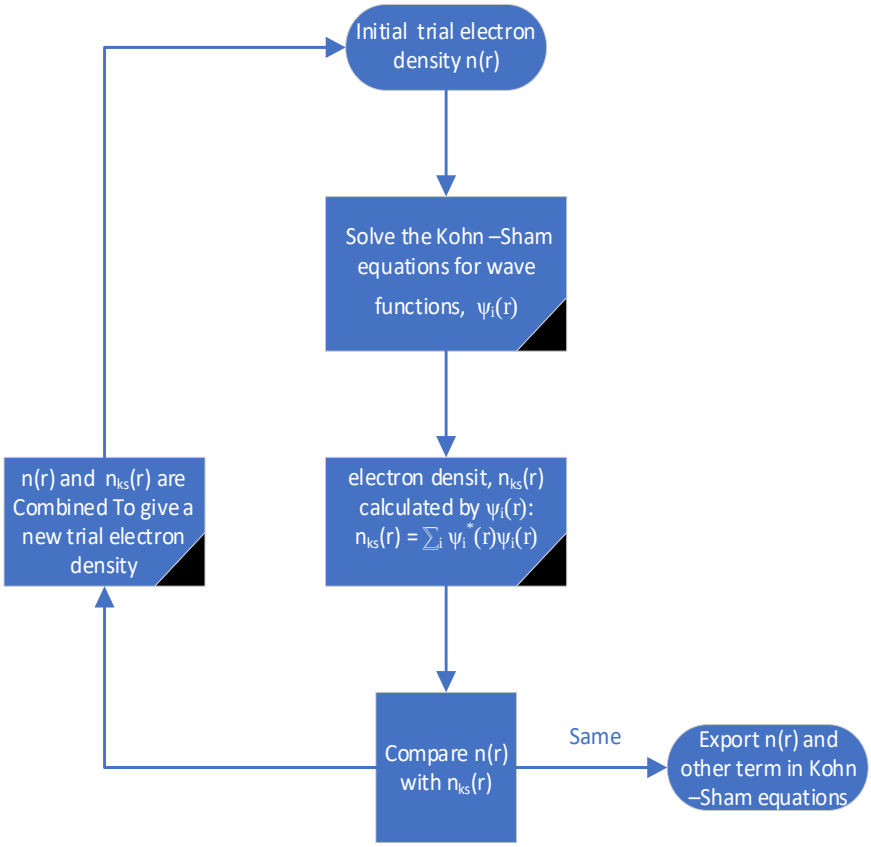

Figure 2.1. The calculation process of first principles

Comparing two solutions for the electron density is the most direct test to determine the stop of iterative calculations, but it could be more convenient. Comparison between total energy and energy corresponding to the electron density could be better way to stop iterative (**Figure 2.2**):

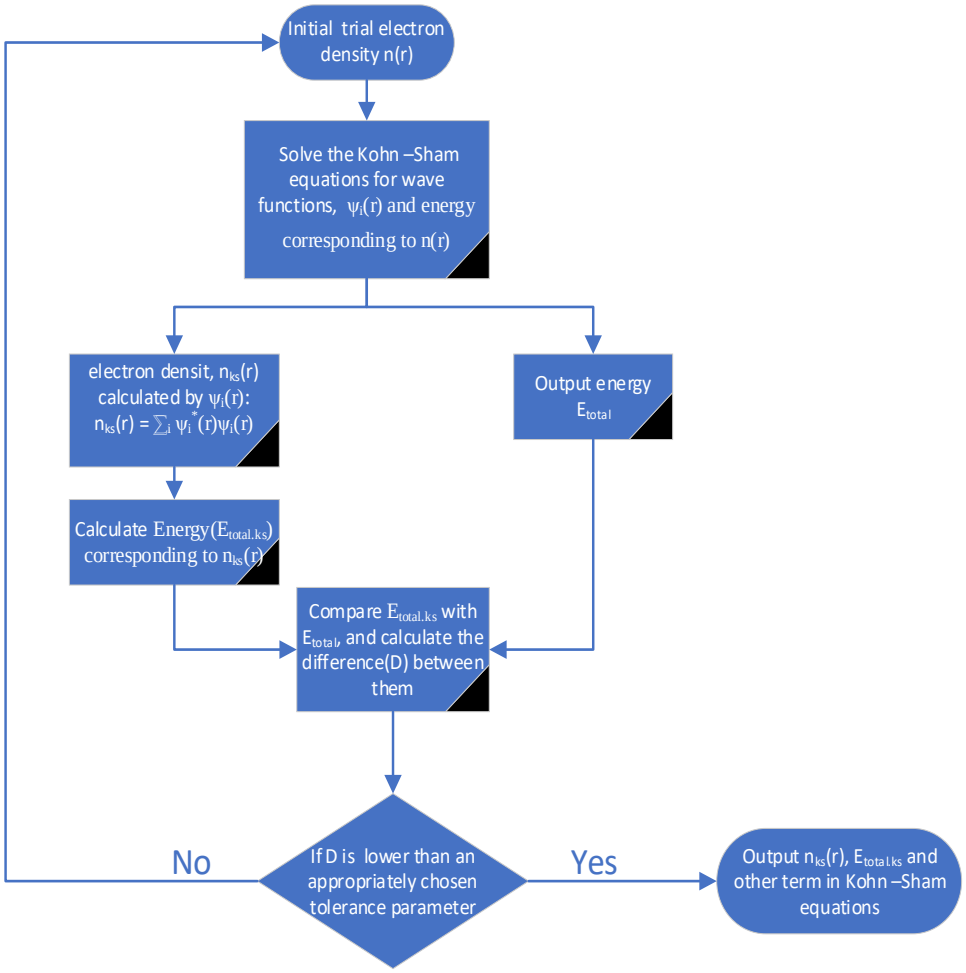

Figure 2.2. The calculated process of first principles in actual calculation

Finally, the focus also needs to return to the formula, Kohn-Sham equations support an excellent way to reduce the cost of computation, but there is a critical complication in the Kohn-Sham equations - how to calculate the Exchange-correction energy $E_{XC}[\{\psi_i\}]$. It cannot be calculated accurately as mentioned above and includes remaining electronic energy from kinetic and electrostatic terms.

2.4 Exchange - Correction Energy and Function

The exchange-correlation energy (E_{XC}) of a many-electron system is the critical quantity of DFT. The accuracy of predictions made using DFT hinges on the precision of the approximation to the exchange-correlation (XC) energy functional, which is typically unknown.[105] E_{XC} per particle could be divided into exchange and correction contributions. The exchange part accounts for the difference between the classical and quantum mechanical electron-electron repulsion; the correction part describes the difference in kinetic energy between the fictitious non-interacting system and the real system.[102, 106] It is not easy to calculate accurately, but it can be calculated approximately. Methods based on Kohn-Sham DFT all need to approximate the unknown actual density functional, and hundreds of approximation functions exist.

Among them, local density approximation and generalized gradient approximation are the most common and primary density function approximations.

2.4.1 Local density approximation (LDA)

LDA was a prevalent functional used by DFT in earlier times, partly due to the error cancellation that occurred among different approximations and its resulting satisfactory performance.[107] LDA assumes a simple form, a linear function of the density, and only local density is used to define the approximate exchange correction function. This formula can describe it:

$$E_{XC}^{LDA} = \int n(r)\varepsilon XC(n(r))dr \tag{2.9}$$

In the equation (9), $\varepsilon XC(n(r))$ is E_{Xc} per electron of a uniform electron gas. Furthermore, $\varepsilon XC(n(r))$ is similar to the overall exchange energy that can be divided into exchange and correction terms. Compared with other approximate calculation functions, LDA is simple and clear. Nevertheless, simplicity does not mean there is bad calculation performance. The LDA functional has exhibited favourable performance in calculating the interaction between molecules and 2-D materials like graphene. However, LDA also has obvious disadvantages, for example, binding energy will be overestimated and bond length will be underestimated by LDA. In the adsorption calculation, LDA could provide a maximum estimate of the adsorption energy.[108]

2.4.2 Generalized gradient approximation (GGA)

GGA is semi-local and considered to improve upon LDA. However, there are more complicated approximations that are nonlocal or orbital-dependent. Their low computational efficiency makes it difficult for them to be widely used in computing. GGA is commonly viewed as a more accurate alternative to LDA due to the incorporation of more physical information, yet this belief is not always substantiated in practical applications.[95, 109]

In a system where the electron density changes rapidly with space, the electron density cannot be spatially uniform as in the ideal case. Hence, the LDA approach has limitations in many cases. Compared to LDA, GGAs depend not only on the density's local value but also on the extent to which the density changes locally. Functionals that depend on the density and gradient of the density are 'gradient corrected', and the existence of 'gradient corrected' defines the 'generalized gradient approximation' (GGA).[106] So, GGA has one more enhancement factor (scaled gradient of the density) than LDA:

$$E_{XC}^{GGA} = \int n(r)\varepsilon XC(n(r))dr + \int F_{XC}(n(r),\ \nabla \mathrm{n(r)})dr \tag{2.10}$$

In the above equation, $\int F_{XC}(n(r), \nabla n(r))dr$ is the scaled gradient, which is the enhancement factor compared with LDA. Because of many ways, which can include the information of electron density gradient (F_{XC}) in the GGA functional, many distinct GGA functionals are created and applied to different types of computing. Moreover, the most widely used GGA functions in the solid calculation are Perdew-Burke-Ernzerhof functional (PBE) and Perdew-Wang functional (PW91).[110, 111]

2.4.2.1 Generalized gradient approximation (GGA) - PBE and PW91

PBE and PW91, both developed by Perdew's group, are typically regarded as interchangeable, with nearly identical results in most cases. However, they have different forms. PBE comes from the simplification of PW91 and has a more concise formula than PW91, which yields almost identical numerical results. PBE also has an advanced version - revised Perdew-Burke-Ernzerhof functionals (RPBE), which may violate the Lieb-Oxford criterion that even modified twice. [112, 113] There are many revised versions of PBE, PBE is the most balanced choice in the calculation.

2.4.3 Dispersion correction and the choice of density function approximation

The poor description of dispersion energy by LDA and GGA also needs to be corrected. Within the scope of this study, several significant elements of DFT analysis, such as adsorption energies, variation in energy gaps, DOS, electron density, and charge transfer, hold crucial importance, with a particular emphasis on adsorption energies. Adsorption energy is essential to describe the adsorption strength, which highly depends on the exchange functional. GGA (underestimate) and LDA (overestimate) are both exchange functional, but would get lower and upper limits of adsorption strengths.[108] The reason for the deviation is suspected to be a bad description of dispersion energy. Dispersion forces are the weakest intermolecular force, yet they contribute significantly to the binding energy in molecules and materials. Therefore, a poor description of dispersion energy in a functional can significantly impact adsorption processes and other calculations. Dispersion-corrected can be implemented in many ways, DFT+D proposed by Grimme’s group is the most widely used.[114, 115] DFT+D dispersion correction is updated many times by Grimme’s group, D3 method is the most widely used and D4 method latest and most accurate. The D3 method cannot calculate the electronic structure. In order to improve the defect that D3 cannot consider the actual electronic structure, D4 method is associated with charge. Due to semi-empirical tight-binding procedure, the computational cost of D4 is greater than the cost of purely geometrical D3 model, but the cost of D4 can be negligible in actual DFT+D calculation that D4 procedure is orders of magnitude faster compared to DFT calculation.[115] Thus, the final functional we choose is PBE-

D4.

2.5 Application of first principles in gas sensing field

First-principles approach is a valuable tool for the prediction of adsorption properties. Theoretical calculations provide a means to discern the atomistic mechanisms underlying gas sensing and delve into the intrinsic modifications taking place within sensing materials. Properties of analysis encompass an analysis of reaction mechanisms, binding strengths, charge transfer, and other electronic and structural features of both the nanomaterials and the interaction with the gas sensors.[23, 94] Adsorption calculations and characterization are primarily centered around the analysis of adsorption energy, charge transfer, charge density difference, band structure, DOS, Electron localization function (ELF), and Natural Orbitals for Chemical Valence (NOCV). Adsorption energy could determine the most stable adsorption configuration, charge transfer determines the sensitivity of ReS_2 to gas. Band structure and DOS show the effect of gas adsorption on the electronic structure of materials. CDD, ELF and NOCV have been entrusted with the responsibility of in-depth analysis of the forces between gases and materials.

2.5.1 Adsorption energy

The adsorption energy serves as a key indicator of adsorption capacity. Calculating the energy difference of a system before and after the adsorption process, allowing the adsorption energy- E_{ad} (Eq (2.11)) can be obtained, allowing for an analysis of molecule stability at various adsorption configurations. The most stable form of an adsorption model can be determined through maximum energy relaxation.

$$E_{ad} = E_{gas-sub} - E_{sub} - E_{gas} \tag{2.11}$$

Where $E_{gas-sub}$ and E_{sub} are the total energy of the 2-D sub before and after gas molecule adsorption and E_{gas} is the energy of the isolated gas molecule before adsorption. Gas adsorption can be deemed spontaneous and favourable when the adsorption energy is negative; conversely, a positive adsorption energy would indicate the difficulty in adsorption.

2.5.2 Charge transfer

Charge transfer between gas molecules and solid surfaces is a critical step in gas-surface reactions, as it influences carrier concentrations and determines the electronic properties of the adsorbent material. Understanding this charge transfer is crucial in designing and optimising materials for various applications, including catalysis,

sensing, and energy storage.

Directly probing the charge transfer on the atomic scale is challenging. A variety of charge analysis methods have been published. Different charge assignment method has their ways of partitioning the electronic density, which causes different numbers for the atomic charges. Mulliken population analysis,[116] Atoms in Molecules (AIM) approach of Bader,[117] Hirshfeld Method,[118] are Charge Model 5 (CM5)[119-121] widely used methods; and Voronoi Deformation density (VDD) method is a particular method supported by software used in the calculation.[122]

Mulliken charge analysis method may produce significant errors in results. It is founded on using base functions to represent the molecular wave function. Bader method is based on the spatial function that defines an atomic domain via topology of the electron density. Hirshfeld Method also relies on electron density as a function of space. Nevertheless, they partition schemes electron density in quite different ways.[123] CM5 is an extension of Hirshfeld Method for Gaseous and Condensed Phases, which is nearly free from dependence on the basis set. A satisfactory agreement between the Hirshfeld charges and the CM5 data can be achieved, except for hydrogens that are bonded to O, N, or P.[119-121]

VDD based on spatial integration of the electron density function over atomic domains, and it does not depend on the projection of the wave function on the basic functions. Like Bader and Hirshfeld methods, VDD is also founded on this fundamental concept. The Voronoi cell has a well-defined boundary and purely geometric definition, while the Hirshfeld cell is fuzzier, taking into account the different sizes of atoms.[122] The VDD atomic domain is defined as a Voronoi polyhedron. Any point in the atomic domain defined as Voronoi polyhedron is closer to atom than any other atom in the system. It can directly measure charge flows caused by chemical interactions into or out of the atoms Voronoi cell. In this thesis, Hirshfeld, Voronoi, CM5 and Mulliken method is employed for charge analysis.

2.5.3 Charge density difference (CDD)

The Charge density difference can obtain the distribution produced by the interaction between adsorbent and adsorbent. The software could plot the charge redistribution due to the adsorption system. The CDD result can describe the magnitude of while interaction and the type of auxiliary determination key.

The CDD calculation formula has the same structure as the formula for adsorption energy. It is the difference comes from the ‘total electron density of the combined adsorbent and adsorbent system’ and ‘densities of the isolated adsorbent and adsorbent system’:

$$\rho_{ad} = \rho_{gas-sub} - \rho_{sub} - \rho_{gas} \tag{2.12}$$

2.5.4 Electron localization function (ELF)

The ELF is a different approach to visualising chemical bonding or interaction. ELF does not depend on the calculation method and the basic sets. The essence of ELF is based on Pauli Exclusion Principle. The sum of N-particle wave function corresponds to a probability density which shows the maximum where the chemist imagines the bonds. However, the wave function needs four quantum numbers brings difficulty, which is similar to the reason why DFT replaced the Schrödinger equation, it is hard to perform in practice. Nevertheless, if the method could be basic on Pauli Principle only need 2 coordinates. In a given region, having electrons with the same spin is challenging. The ELF could support a measurement of the probability of finding identical spins electrons in a space region. The result from ELF is mapped onto the range [0 ,1], which is compared to uniform electron gas with the same density:

$$ELF = \frac{1}{1+\chi_\sigma^2} \tag{2.13}$$

The χ_σ is the electron localization ratio of the measurement system (D_σ) and uniform electron gas (D_σ^0):

$$\chi_\sigma = \frac{D_\sigma}{D_\sigma^0} \tag{2.14}$$

The measured electron gas corresponds to the uniform electron gas when ELF is equal to 0.5, and the measured electron gas has been perfect localization when ELF is equal to 1.[124-126] ELF can indicate the charge redistribution and bonding nature of the adsorbed gas molecules on a surface

2.5.5 Density of state (DOS) and Band structure

DOS and Band structure are the key factors in condensed matter physics and material science. They could observe the electronic structure and determine electronic properties. The study of electronic properties in adsorption systems, and comparison with the electronic properties of individual adsorbent materials, can provide a clear understanding of the impact of gas adsorption on materials and whether they can serve as electronic component materials for adsorbing gases.

DOS is a crucial concept in solid-state physics as it quantifies the number of available states at a particular energy level. It can also be expressed as the number of electron states per unit volume. By examining the DOS, we can directly determine the band gap of a material. Additionally, a deeper analysis of the DOS (known as the

partial density of states, or PDOS) can reveal valuable information about the hybridization of orbitals and the nature of bonding between atoms.

While the DOS provides essential information about a material's electronic properties, the band structure offers a more nuanced and detailed view of its electronic structure. The band structure displays the energy of available electronic states along an enclosed path in reciprocal space.[127] One way to think of the DOS is as an observational perspective of the band structure. Gas adsorption can induce significant changes in the electronic structure of a material, particularly in the band gap, which is advantageous for gas sensors as it alters the electrical signal output, allowing for the detection and quantification of specific gases.

2.5.6 Natural Orbitals for Chemical Valence (NOCV)

It is typical to evaluate and break down the adsorption energy into various components before conducting a NOCV (Natural Orbitals for Chemical Valence) analysis, as the adsorption energy is a fundamental parameter in determining the strength of the bond between a molecule and a surface. NOCV can provide an intuitive and visual representation of orbital interactions. Orbital interactions involve orbital mixing and relaxation, charge transfer, and polarization. NOCV and CDD can complement each other by offering different insights into the nature of chemical bonding. NOCV primarily examines the orbital interactions and energy contributions of each bond component, whereas CDD focuses on the net charge displacement and polarization effects. Combining these perspectives can achieve a more comprehensive understanding of how atoms form bonds and share electrons.

In this thesis, the adsorption energy (ΔE_{int}) was quantified using Energy Decomposition Analysis (EDA), which allows for determining of the contributions of various energy terms to the overall interaction. The ΔE_{int} is contributed multiple compositions, including electrostatics energy (ΔE_{elstat}), Pauli repulsion (ΔE_{Pauli}), orbital interactions (ΔE_{oi}) and dispersion energy (ΔE_{disp}, only the calculation uses dispersion correction). NOCV is a further energy analysis focusing on orbital interactions. Orbital interactions involve orbital mixing and relaxation, charge transfer, and polarization. The contribution of pairs of complementary orbitals to total orbital interaction is partitioned and analysed by NOCV. In software, we applied NOCV and energy decomposition analysis to analyse the orbital term, which is expected to be decomposed and transformed into intuitive chemically meaningful contributions.

2.5.7 Extra electric field

The gas sensing properties of single-layer materials may be sensitive to the extra electric field. In many calculations, the external electric field has been verified that has an effect on the adsorption properties of gas molecules. The properties affected include action strength, orbital overlapping and charge transfer between gas and

materials.[128, 129] The extra electric field is set from 1 V/Å to -1 V/Å, which is perpendicular to the plane of monolayer ReS_2. Furthermore, the electric field is applied in the most stable configuration which from optimisation of adsorption configuration.

2.6 Software and Calculation process

2.6.1 AMS

The software used in this study is the Amsterdam Modeling Suite (AMS), which has been employed wildly in the areas of chemistry, materials science, and engineering. It includes multiple program codes, such as ADF, BAND, DFTB and ReaxFF. DFTB module is responsibility for reducing computing costs via pre-optimisation before BAND. Compared to the plane wave program, the 2-D material is an actual 2-D model in BAND and DFTB programs, which shows high reliability and efficiency of surface adsorption calculation.[130-134]

2.6.2 Modules

2.6.2.1 DFTB

DFTB is used for pre-optimisation of adsorption configuration before BAND module calculation to reduce the cost of time. It only requires a fraction of the computational cost of DFT calculations while providing relatively accurate results. This is achieved by using pre-calculated parameters, a minimal basis, and considering only nearest-neighbour interactions. Only the Generalized Force Field 1st Order Tight Binding (GFN1-xTB) function can be used, as the other functions have been parametrized separately. It is crucial to specify the appropriate matching parameter set when applying any of these models. The DFTB engine supports the GFN1-xTB parameterization of xTB, which is specifically optimised for geometries, frequencies, and non-covalent interactions. It covers almost all elements (atomic number=1−86) of the periodic table, including radon. GFN1-xTB is a highly robust and widely applicable semiempirical quantum chemical method for calculating the structures, vibrational frequencies, and noncovalent interactions of molecules across the periodic table.[135] When using the GFN1-xTB model Hamiltonian, the D3-BJ dispersion correction is automatically enabled by default.

2.6.2.2 BAND

The BAND is the main module used in the calculation for the study of gas sensing properties of 2-D materials. BAND module will perform the optimisation and analysis of most adsorption configuration. The BAND use atomic orbitals for periodic DFT

calculations, which has advantages in studying low-dimensional periodic materials. There is no c-axis in the slab period in BAND, so interlaminar forces need not be considered. For the XC function we can choose PBE-D4 and LDA in BAND module.

2.7 The target gas for analysis

The target gases are common small hazardous gas - CO, CO_2, NO, NO_2 and H_2. NO_2 adsorption on ReS_2 has been experimentally and theoretically calculated. The experiment and calculation both show ReS_2 has high sensibility to NO_2. Our calculation of NO_2 can serve as a validation and supplement to the calculations in previous articles, and the NO_2 data can also be used as a standard for comparing the adsorption results of the other four gases. Other four gas are common small molecule industries and dangerous gases.

Chapter 3

ReS_2 - Optimisation and Analysis

3.1 Synopsis

The ReS_2 is a crystal that has not attracted much attention by experiment and computation. To start with, this chapter focuses on optimising and analysing the 2-D ReS_2 structure.

Establishing and characterising the crystal structure of monolayer ReS_2 is a crucial step before performing gas adsorption calculations. The optimised monolayer ReS_2 can provide valuable insights into the material's adsorption properties for different gas molecules. We employ the BAND module in the AMS software to optimise and analyze the properties of 2-D ReS_2 using 2-D periodic systems, focusing on displaying the resulting lattice parameters and electronic properties.

3.2 The ReS_2 crystal file and computational details

The ReS_2 CIF document available on 'Materials Project' pertains to 3D ReS_2, and data in CIF are based on theoretical calculations.[136] The 'Calculation Summary' on the website provides clear information about the optimisation process used to obtain the documented crystal structure. The structure optimisation of ReS_2 was carried out using the VISP projector augmented wave method, with a cutoff energy of 520 eV. The final energy per atom obtained was - 7.4744 eV. The lattice parameters specified in the ReS_2.cif file are a = 6.419 Å, b = 6.523 Å, and c = 7.045 Å.

The optimisation and analysis of 2-D ReS_2 were carried out using the BAND module with Slab Periodicity prior to adsorption calculations. The optimisation process involved gradient analysis with the PBE exchange-correlation functional. For the system, the basis set verified DZP. However, due to the presence of heavy Re atoms, the TZ2P basis set was exclusively used for Re atoms.

Geometry optimisation is performed using the gradient descent approach with the convergence criterion of 0.001 Hartree/Å for the gradient, 10^{-5} Hartree for the potential energy. 0.01 Å for the distance and 0.0005 Hartree Stress energy per atom. The k-point mesh for Brillouin zone integration is determined by the size of a lattice vector and the K-Space quality. In this calculation, k-point grid parameters are set to 'very good' and are at least or larger than 21 × 42 × 1.

The optimised 2-D ReS_2 will be the adsorption substrate in the adsorption calculation. Therefore, the ReS_2 will be analysed before adsorption configuration optimisation with target gases. The analysis process is also run using the BAND module with PBE functional.

3.3 ReS_2 Optimisation results and analysis results

3.3.1 ReS_2 optimised model and lattice constant

The crystal structure of ReS_2 is different from most TMDs structures. The optimised results of 2-D ReS_2 are shown with MoS_2 and HfS_2 in **Figure 3.1** for comparison. MoS_2 and HfS_2 represent the TMDs with 1-H structure and 1-T structure, while ReS_2 shows a deformity 1-T structure. **Figure 3.2** shows the unit cells of the three materials. It can be observed that the ReS_2 unit cell is relatively larger than other TMDs members' cells. The lattice constant of the optimized ReS_2 structure is computed. The lattice constant is a = 6.411Å, b = 6.544Å and γ = 118.872°, which are which is very close to the experimental value of a = 6.42 Å, b = 6.52 Å.[137] The area of ReS_2 cell is 36.738$Å^2$. Because of Slab Periodicity (2-D model), the lattice does not show a c-axis constant and only monolayer existence.

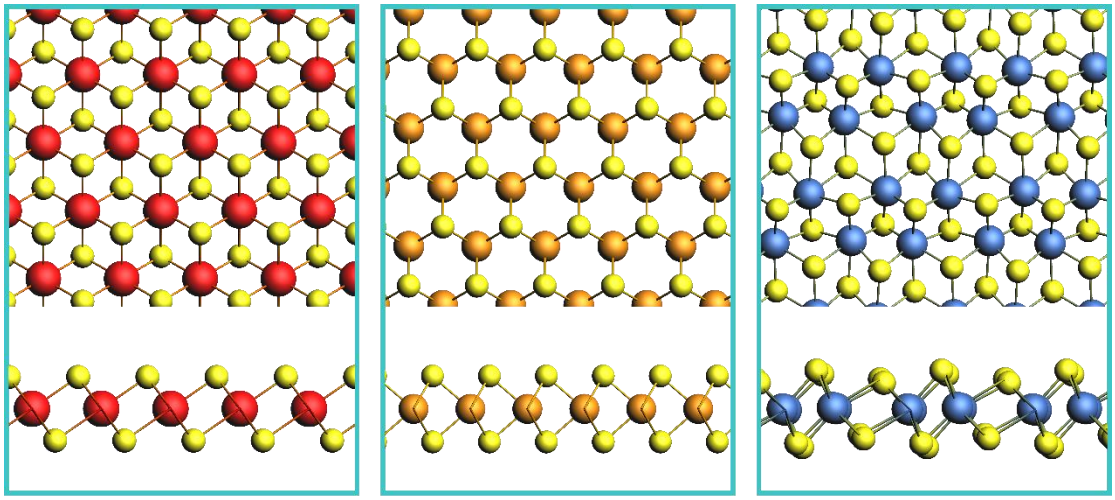

Figure 3.1. Vertical view and lateral view (a) HfS_2 with 1-T structure, (b)MoS_2 with 1-H structure, (c)ReS_2 1-T' structure

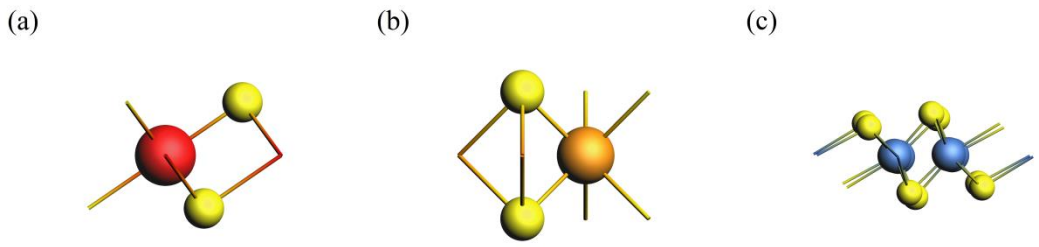

Figure 3.2. Unit cell of (a) HfS_2, (b)MoS_2 and (c) ReS_2

The pristine ReS_2 monolayer shown in **Figure 3.3** is notable for the presence of zigzag Re chains, which are highlighted by red lines. This distortion in the crystal structure results from the additional electron per Re atom that occurs during the crystal formation process. The Re chains are also responsible for influencing the formation energy of the material, as the strong covalent bonding between Re atoms in the chains contributes to the high formation energy of the ReS_2. The formation energy of ReS_2 is among the highest for TMDs with stable structures. The solid formation energy of ReS_2 cell is -88.6868 eV, which translates to -7.391 eV per atom. This value is consistent with previous studies and suggests that ReS_2 has a stable structure.[89] In contrast, other members of the TMDs class, such as MoS_2 (-5.110 eV/atom) and WS_2 (-5.693 eV/atom), have lower cohesive energy.[138] The presence of Re chains in 2-D ReS_2 reduces the overall energy of the material while also contributing to significant anisotropy within the plane.

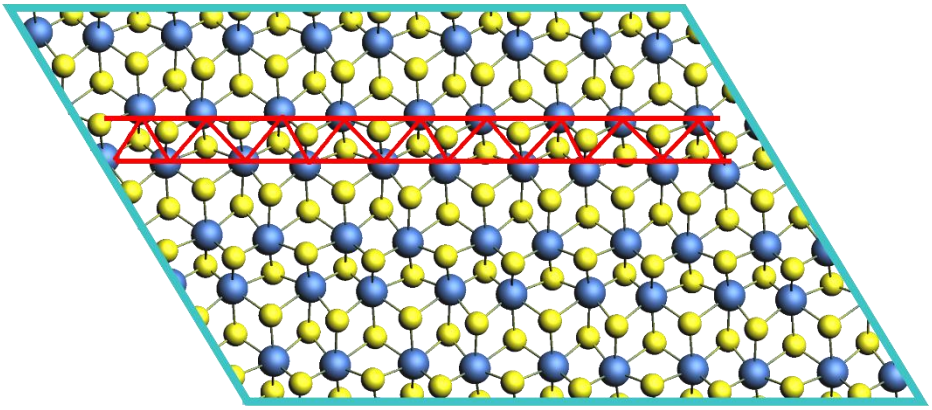

Figure 3.3. Monolayer ReS_2 vertical view. The red line describes one Re chain.

3.3.2 Electronic properties of ReS_2

Calculating the electronic properties of ReS_2 is essential for comparing its properties with those of adsorbents and adsorbent systems, and for assessing its

suitability as an electronic component material. By comparing the electronic properties of ReS_2 before and after gas adsorption, we can determine if there are significant changes in its properties and how these changes affect its gas adsorption behaviour. The main electronic properties that are typically analysed for ReS_2 include the DOS and the band structure, as these properties provide insights into the electronic behaviour of the material and its interaction with gas molecules.

The most crucial expression of electronic properties is the Band structure (**Figure 3.4**). In addition, fat band analysis is also calculated and shown in the band structure by colours, which can give the main components of each section of the energy band curve. Because of the deformed structure, the K-point path for ReS_2 band structure analysis is not a single circuit connected head to tail. It is automatically generated by the BAND module to find as many symmetry points as possible. The band structure is not continuous in the middle. K-path is from A_1 to Γ and then divided into two paths (Γ-A_2 and Γ-A_3).

The band gap is the minimum energy difference between the valence band (VB) and the conduction band (CB). It needs the highest point of VB and the lowest point of CB. A direct band gap material has an aligned minimum value of the conduction band and maximum value of the valence band. In the band structure, we can get the band gap in the Γ point. The direct band gap material has aligned the minimum value of the conduction band and the maximum value of the valence band. **Figure 3.4 (a)** provides clear evidence that ReS_2 is a direct band gap semiconductor material with a band gap of 1.421 eV that appears at the Γ point. The value of the band gap obtained in this study for ReS_2 is consistent with the data reported in literature.[89, 137]

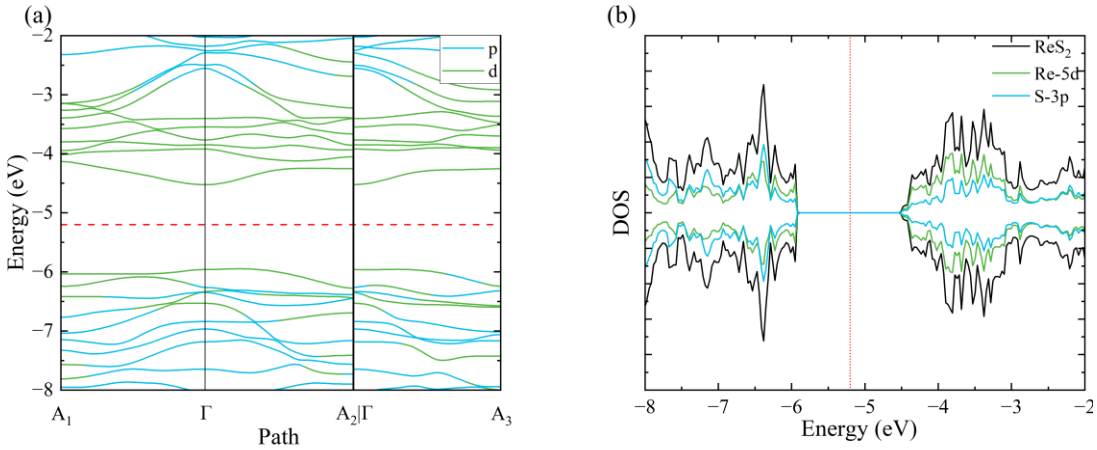

Figure 3.4. (a) Band structure and (b) DOS of ReS_2 monolayer.

The Fermi energy level, denoted by the red line in the band structure and DOS, lies within the bandgap between the valence and conduction bands. It is typically calculated by software that uses an energy reference point of infinity with zero vacuum energy. The Fermi energy level has practical physical significance, and its absolute value can represent the work function of 2-D materials. The work function,

on the other hand, represents the energy required to remove an electron from the Fermi level and prevent it from escaping the solid. For 2-D-periodic metal systems, the work function can be determined by taking the difference between the Fermi energy and the vacuum energy (0 eV). For ReS_2, Fermi energy is -5.20 eV; thus, the work function is calculated to be 5.20 eV in this study.

The full electron configuration of Re element is $2s^2$ $2p^6$ $3s^2$ $3p^6$ $3d^{10}$ $4s^2$ $4p^6$ $4d^{10}$ $4f^{14}$ $5s^2$ $5p^6$ $5d^5$ $6s^2$ and S element is $1s^2$ $2s^2$ $2p^6$ $3s^2$ $3p^4$. The fat analysis content can provide valuable information about the composition of CBM, d and s orbitals have the greatest contribution to valence band maximum (VBM) and conduction band minimum (CBM). This is consistent with the conclusion of previous studies.[139] Re atoms 5d orbitals and S atoms 3p orbitals contribute VBM, and Re atoms 5d orbitals contribute CBM. The DOS analysis (**Figure 3.4 b**) also supports this point. DOS shows the number of electron states per unit volume per unit energy which is easier for visualization than the band structure data. Generally, DOS can be regarded as another perspective of the band structure. In the DOS, the Fermi level also locates at the red line, which is the same as the value in the band structure. Compared to fat band analysis, the DOS can exhibit subshells. In **Figure 3.4 (b)**, subshells of Re atoms 5d and S atoms 3p are both shown. Their contribution to CBM and VBM is clearly shown in the figure. Re atoms 5d made great contributions to both VBM and CBM, S atoms 3p orbitals only have a huge peak near VBM. Meanwhile, by fat analysis, p orbitals show that they only contribute a short section to VBM. Thus, Re-5d is the main contributor to CBM and VBM. Finally, regarding location, VBM and CBM are located at the Highest Occupied Crystal Orbital and Lowest Unoccupied Crystal Orbital.

3.4 Summary

Optimizing and analysing ReS_2 is fundamental to gas adsorption calculation since it is the adsorbent material that will be studied in future research. In this chapter, ReS_2 was optimized in 2-D periodicity, and interlayer interaction was not considered. The lattice constant and properties of ReS_2 were analysed using the BAND DFT package.

The analysis of ReS_2 is crucial in comparing it with the properties of the most stable adsorption configurations in the next chapters. Specifically, electronic properties such as DOS and band structure are important to consider.

Chapter 4

Optimisation and analysis of CO_2, CO and H_2 adsorption configuration on ReS_2

4.1 Synopsis

This chapter investigates the interactions between CO, CO_2 and H_2 and ReS_2 using first-principles calculations based on DFT. The study is divided into two distinct stages, namely, the optimisation process and the analysis process. The purpose of the optimization process is to find a stable adsorption structure. In the analysis process, the most stable configuration will be determined by conducting a comparative evaluation of the adsorption energy, followed by a comprehensive examination of additional adsorption characteristics. To guarantee the identification of the most stable configuration, it is imperative to consider multiple active sites as initial locations and initial configurations in the optimisation process, serving as the initial configuration of the gas molecules. The resulting configuration and adsorption properties shall furnish a theoretical foundation for the future experimentation and implementation of ReS_2 in the realm of gas sensing.

4.2 Introduction

Air pollution is a global issue that has been extensively discussed in various environmental conferences and international communications. Among the various greenhouse gases, CO_2 is the most notorious, accounting for 77% of greenhouse gas emissions caused by human activities and is responsible for contributing to global warming. Combustion of fossil fuels is the main source of CO_2 emissions, with total world CO_2 emissions reaching about 34 million kilotons in 2019, according to data from The World Bank.[140] Detecting anthropogenic CO_2 emissions is crucial due to its significant role in long-term climate change. Moreover, high levels of CO_2 in the environment can adversely affect human health, leading to severe conditions such as cardiac arrhythmias, seizures, and anoxia due to severe acidosis.[14, 17] So, processes involved in CO_2 detection for emissions and leaks have gained attention in the scientific community, whether in sinks dominating the carbon cycle or industrial production environment.

Compared to CO_2, CO has more direct harm to human. CO is produced when carbon-based compounds are incompletely burned, and is a colourless, odourless, tasteless gas that can be highly toxic at high concentrations. It is known as a "silent killer" because of its insidious nature. CO could combine with hemoglobin to produce carboxyhemoglobin that can no longer be used for oxygen transport in the body, and the CO binds to haemoglobin about 200-times more strongly than Oxygen that can reduce the oxygen-carrying capacity of the blood. CO intoxication can present a wide range of acute and chronic symptoms, including dizziness, myocardial ischemia, pulmonary edema and so on. Therefore, CO intoxication lacks a unique clinical signature. CO poisoning can have severe and even fatal consequences, with more than half of the world's fatal poisonings being attributed to CO.[19, 141-143] CO detectors have a variety of sorts, but they are still limited by high cost, low sensitivity and low portability. Thus, to improve health and safety, research of new CO gas sensing materials is indispensable.

H_2 plays a crucial role in industrial processes and is distinct from CO_2 and CO. With advancements in hydrogen energy utilisation technology, hydrogen has emerged as a promising clean and renewable energy source that can replace fossil fuels. The implementation of H_2 as a fuel source offers numerous benefits for both industry and everyday life. Hydrogen refueling stations are popular investment projects, but they are close to civilian living quarters. However, it is important to acknowledge the potential danger associated with H_2. The boiling point and ignition energy of hydrogen are extremely low, and it is highly flammable. The leakage of gaseous hydrogen will quickly spread out of a hydrogen cloud with a large range, due to high storage pressure. The flammable and explosive hydrogen cloud will become a hazardous region and may cause large-scale disasters. Therefore, gas sensors with sensitive, short response time and low LOD is essential and urgent to ensure safe hydrogen storage and protect human safety.[144, 145]

The objective of this chapter is to calculate the adsorption properties and configurations of three gases on ReS_2. The calculated data are the basis for future experiments and applications. The calculation starts from initial configuration and site selection: (i) there are five active sites and (ii) initial configuration quantity depends on the gas itself. The next step is configuration optimization. Each initial configuration located above different active sites needs to be optimised. All optimised configurations need to be analysed to obtain adsorption energy and charge transfer properties. Out of all the results, the configuration with the highest absolute value of adsorption energy is the desired outcome. The adsorption energy serves as an indicator of the strength and stability of the adsorption configuration. Adsorption energy may be a positive or negative value. Positive adsorption energy indicates that the total energy of the system increases after adsorption, making adsorption less likely to occur. Negative adsorption energy is considered stable, as it results in a reduction of the total energy of the adsorption system. The stability of the adsorption configuration increases with the absolute value of the adsorption energy. The most

stable configuration will be characterised for various properties of adsorption. These properties can reflect the changes in the system before and after the gas adsorption, the properties of the bond between the adsorbent and the adsorption, and the changes of the electrical properties in the adsorption material.

4.3 Simulation Details

The quality of the results of a computer simulation in DFT calculation mainly depends on the Exchange - Correction Energy functional and K-space for a periodic system. PBE-D4 is a reasonable choice for optimization and analysis of gas adsorption configuration due a robust dispersion energy correction. It will be the main functional for our calculations. LDA funtionals, on the other hand, has less accurate than PBE-D4 but can provide an upper limit of adsorption energy and takes less time than PBE-D4. Optimization and analysis mainly run using the BAND package with either LDA or PBE-D4 functional. To reduce computing time, DFTB modules are employed for pre-optimisation.

The initial configuration to be optimised should consider the active point and configuration of the gas. There are five active sites on ReS_2 unit cell, called P1, P2, P3, P4 and P5 (**Figure 4.1**):

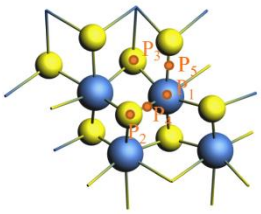

Figure 4.1. Active sites above ReS_2 monolayer: P1, P2, P3, P4 and P5.

The gas molecule is located at active sites above the surface of the ReS_2 material site with 2.5 Å distance between the gas and the surface. Except for the initial position, different gas configurations also need to be considered. Molecular structures of CO_2, CO and H_2 are very different, so their initial configuration needs to be considered separately. Of course, the primary gas configurations are parallel to and perpendicular to the material. Based on these two, consider the influence of gas structure on configuration.

All initial gas position and configurations need to be optimized to ensure the most stable adsorption configuration of gas and materials are obtained. Pre-optimization in DFTB is used before the optimisation in BAND. We use the GFN1-xTB method for all calculations. Pre-optimization in DFTB requires only a fraction of the cost of DFT calculation for relatively accurate results. After pre-optimization, the optimization

continues in BAND with LDA and PBE-D4. LDA is first used, and PBE continue to optimize the result from LDA.

Before the optimisation process, parameters need to be set. In the BAND module, the DZP basis set is checked for the system, and the TZ2P basis set is solely checked to be used for Re atoms. The geometry optimisation by gradient method follows the convergence criterion of 0.001 Hartree/Å for gradient, 10^{-5} Hartree for the potential energy, 0.01 Å for step convergence, and 0.0005 Hartree for stress energy per atom. In this study, the k-point mesh used for Brillouin zone integration in the software is determined based on the size of the lattice vector and the desired quality of the K-Space. The K-Space quality was set to "very good". The logfile shows that the k-space number used for adsorption calculation was at least 21 x 42 x 1 or larger.

Analysis of the optimised structures is also performed using the BAND module. The adsorption energy is first computed for the most sable configurations, followed by other adsorption properties, including charge transfer, charge density difference, DOS, and band structure.

4.4 Result and Discussion

4.4.1 Most stable configuration

The value of adsorption energy directly reflects the adsorption strength. The adsorption energy for each adsorbate correspond to its favorable adsorption configurations obtained above different sites with different initial gas configurations. The most stable configuration can be identified by the largest adsorption energy. Study summarises the adsorption energy data for the initial configurations after optimisation, adsorption systems for CO, CO_2, and H_2 are listed separately in **Tables 4.1**, **4.2**, and **4.3**, respectively. All adsorption energies are negative, energy of the system after adsorption is lower than that before adsorption. These can prove that the adsorption of three gases on ReS_2 is spontaneous.

Table 4.1 Adsorption energy of CO adsorption configuration.

		Adsorption energy(eV)	
Active site	Initial configuration	LDA	PBE-D4
P1	Parallel	-0.329	-0.241
	C atom above O atom	-0.357	-0.259
	O atom above C atom	-0.267	-0.225
P2	Parallel	-0.336	-0.251
	C atom above O atom	-0.238	-0.197
	O atom above C atom	-0.355	-0.179
P3	Parallel	-0.357	-0.259
	C atom above O atom	-0.357	-0.223
	O atom above C atom	-0.335	-0.253
P4	Parallel	-0.336	-0.251
	C atom above O atom	-0.354	-0.258
	O atom above C atom	-0.336	-0.251
P5	Parallel	-0.356	-0.26
	C atom above O atom	-0.356	-0.259
	O atom above C atom	-0.356	-0.264

Table 4.2 Adsorption energy of CO_2 adsorption configuration.

		Adsorption energy(eV)	
Active site	Initial configuration	LDA	PBE-D4
P1	Parallel	-0.307	-0.29
	Perpendicular	-0.282	-0.267
P2	Parallel	-0.298	-0.293
	Perpendicular	-0.295	-0.286
P3	Parallel	-0.297	-0.247
	Perpendicular	-0.299	-0.282
P4	Parallel	-0.278	-0.267
	Perpendicular	-0.3	-0.293
P5	Parallel	-0.278	-0.268
	Perpendicular	-0.3	-0.293

Table 4.3 Adsorption energy of H_2 adsorption configuration.

		Adsorption energy(eV)	
Active site	Initial configuration	LDA	PBE-D4
P1	Parallel	-0.097	-0.071
	Perpendicular	-0.091	-0.062
P2	Parallel	-0.085	-0.059
	Perpendicular	-0.081	-0.062
P3	Parallel	-0.082	-0.064
	Perpendicular	-0.068	-0.059
P4	Parallel	-0.088	-0.067
	Perpendicular	-0.071	-0.064
P5	Parallel	-0.091	-0.064
	Perpendicular	-0.096	-0.065

While LDA is utilized for pre-optimisation and to estimate the upper limit of adsorption energy, the main focus of this study is on the results obtained using PBE-D4. Some initial configurations will get the same stable configuration by optimisation. In cases where the optimisation results of two initial configurations yield the same maximum adsorption energy, their respective adsorption configurations are compared to determine whether they are similar or identical.

Table 4.4 summarises the data for the most stable configurations from **Tables 4.1-4.3**, which are also presented as images in **Figure 4.2**. The "Nearest atoms" and "Distance" values in **Table 4.4** are obtained from the PBE-D4 results, as are the configuration images.

Table 4.4 Adsorption properties of CO, CO_2 and H_2 most stable adsorption configurations. (1) Adsorption energy calculated by LDA and PBE-D4 XC function. The negative energy means energy is released in adsorption. (2) Nearest atoms between gas and ReS_2 and (3) Distance(D) between nearest atoms.

Gas	Adsorption energy (eV)		Nearest atoms	D(Å)
	LDA	PBE - D4		
CO	-0.357	-0.264	O-S	3.076
CO_2	-0.307	-0.293	C-S	3.136
H_2	-0.097	-0.071	H-S	3.006

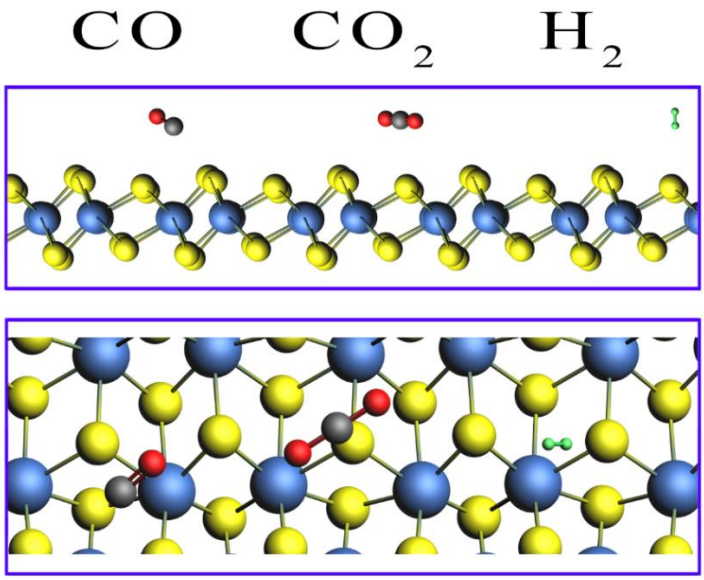

Figure 4.2. Top view and side view of CO, CO_2, H_2, NO_2 and NO adsorption system**.** The direction shown in the side view is consistent with the extension direction of Re chain. The top view shows the region between the two Re chains. In the gas molecule, green atom is hydrogen, red atom is oxygen and grey atom is carbon.

In the table, the results of adsorption energy absolute value from LDA are significantly larger than from PBE-D4. CO and CO_2 show adsorption energy absolute value which are -0.264 eV and -0.293eV. H_2 has the minimum adsorption release energy which is only -0.071 eV. In addition, their distance to nearest ReS_2 atom are all longer than 3 Å. The adsorption energies of NO_2 and CH_3COCH_3 on ReS_2 were reported as -0.65 eV and -0.43 eV, respectively, in a previous study.[89] While ReS_2 was found to be only highly selective to NO_2 in that study. The adsorption energies of all three gases on ReS_2 are relatively lower than NO_2 and CH_3COCH_3, indicating that the adsorption configuration may not be very stable. It is possible to infer that ReS_2 may not be suitable for CO, CO_2 and H_2 detection due to its lower adsorption energy release and stability level, which makes it difficult for the gas molecules to attach to the ReS_2 monolayer. However, more adsorption properties need to be analysed to support this inference.

In **Figure 4.2**, the most stable adsorption configurations calculated by PBE-D4 of gas molecules are all located between Re-chains. The reason for this phenomenon is due to the Re chain part has low whole energy that is unfavourable to the adsorption. Meanwhile, side view and 'Nearest atom' show three gas molecules do not touch the upper surface of the material. The distance between the H_2 molecule and the nearest S atom in ReS_2 monolayer is 3.006 Å, which is the shortest in these gas molecules. CO and CO_2 have longer distance between them and the S atom. The following analysis of adsorption properties are also based on adsorption configurations in **Figure 4.2** by using the PBE-D4 functional.

4.4.2 Charge transfer

Charge transfer is crucial in evaluating the interaction between gas molecules and adsorbent surfaces during the adsorption process. The charge transfer occurs on the surface of 2-D layered nanomaterials when gas molecules are exposed on 2-D layers, which may result in modulation of overall conductivity (resistivity) of 2-D sensing layers. However, the sensitivity of materials to gases requires more understanding of the real impact of gases on electronic structures.

Tables 4.5, **4.6** and **4.7** display the atomic charge transfer values of gas molecules. Only the most stable configuration is analysed here. Charge transfer between adsorbates and absorbents is a crucial step in gas-surface reactions influencing the carrier concentrations of materials. Directly probing the charge transfer on the atomic scale is challenging.

Table 4.5 Charge transfer in CO adsorption configuration. Negative value represents charge from gas molecule to ReS_2. Positive means charge from ReS_2 to gas molecule.

Methods for Charge	Single gas molecule (e)		Gas in adsoprtion system (e)		Transfer(e)
	C	O	C	O	
Hirshfeld	0.082	-0.082	0.065	-0.086	-0.021
VDD	0.091	-0.091	0.086	-0.085	0.001
CM5	0.124	-0.124	0.107	-0.129	-0.022
Mulliken	0.342	-0.342	0.333	-0.327	0.006

Table 4.6 Charge transfer in CO_2 adsorption configuration. Negative value represents charge from gas molecule to ReS_2. Positive means charge from ReS_2 to gas molecule.

Methods for Charge	Single gas molecule (e)			Gas in adsoprtion system (e)			Transfer(e)
	C	O	O	C	O	O	
Hirshfeld	0.284	-0.142	-0.142	0.263	-0.145	-0.144	-0.026
VDD	0.318	-0.159	-0.159	0.305	-0.149	-0.149	0.007
CM5	0.363	-0.181	-0.181	0.342	-0.186	-0.185	-0.03
Mulliken	0.927	-0.463	-0.463	0.876	-0.454	-0.453	-0.032

Table 4.7 Charge transfer in H_2 adsorption configuration. Negative value represents charge from gas molecule to ReS_2. Positive means charge from ReS_2 to gas molecule.

Methods for Charge	Single gas molecule (e)		Gas in adsoprtion system (e)		Transfer(e)
	H	H	H	H	
Hirshfeld	-0	0	-0.029	-0.012	-0.041
VDD	-0	-0	0.004	-0.003	0.001
CM5	-0	0	-0.027	-0.011	-0.038
Mulliken	0	-0	0.048	-0.039	0.009

VDD, Hirshfeld, CM5 and Mulliken charge method are all used for atomic charge analysis in this study. Hirschfeld is the major charge analysis method discussed in this article, VDD could support a reasonable general insight due to its pure mathematical space partition. Charge analysis of gas molecule, whatever any methods, actually show the deformation charges of atoms in the system with respect to neutral.

Charge transfer is from difference of molecular charge before and after optimisation of adsorption configuration. Charge transfer results of three gas adsorption systems is low, the largest of them is H_2 which has -0.041e transfer. CO and CO_2 adsorption have similar results, which are -0.021e and -0.023e. Their charge transfer results are not large, these means the current change in gas sensitive materials is not too large during adsorption. The low transfer is weakness of sensitive materials to these three kinds of gas.

In addition, comparative of charge analysis methods is also interested. In the analysis of single gas, VDD get results is most similar to the Hirshfeld method. The difference between their charge analysis results of single gas is ±0.01e. However,

when analysing the charge distribution of gas molecules in adsorption systems, VDD and Hirshfeld methods may yield different results, leading to a significant difference in the final charge transfer data. While VDD has been proven to be unsuitable for fragment charge analysis calculations due to weak interactions that result in small charge redistributions.

CM5 and Hirshfeld method could get similar results of charge transfer, although their analysis results of atom charge are not inconsistent. CM5 method charge transfer result of CO, CO_2 and H_2 are -0.022e, -0.03e and -0.038e which is near to Hirshfeld results. However, charge analysis data from CM5 and Hirshfeld are not same, even VDD can support a result for single molecule closer to Hirshfeld method's than results from CM5. Take charge analysis of CO as an example, the charge of single gas molecule atoms from Hirshfeld (C atom: 0.082e, O atom: -0.082e) and VDD (C atom: 0.091e, O atom: -0.091e) are close to each other, and CM5 support a value (C atom: 0.124e, O atom: -0.124e) that about 150% of Hirshfeld analysis value. Then, the charge of molecule in the adsorption system should also be compared. CM5 support a value (C atom: 0.107e, O atom: -0.129e) that about 150% of Hirshfeld analysis value (C atom: 0.065e, O atom: -0.086e). Meanwhile, VDD in the fragment calculation shows results (C atom: 0.086e, O atom: -0.085e) that are quite different from Hirshfeld analysis. CM5 method has same trend of charge analysis on gas before and after adsorption configuration optimisation. So, their final transfer results have approximate value. Mulliken is the only method that based on the wave function representation in the table, and its results stay away from other results from CM5, Hirshfeld and VDD method.

4.4.3 Charge density difference (CDD)

Charge density displays density of electrons in the space around materials. Difference in charge densities could show the change trend of electron density distribution outside atoms of a system. In the CDD, we can clearly see the charge transfer phenomenon. CDD could be a crucial parameter that plays a key role in determining the properties and strength of the interaction between the adsorbent and the adsorbate.

In this thesis, CDD is calculated by the charge density of the adsorption system minus the charge density of isolated materials and gases. The CDD for three gas molecules adsorption is shown in **Figure 4.3 (a)**, **(b)** and **(c)** in the figure are respectively CDD of CO, CO_2 and H_2 most stable adsorption configurations. Three pictures clearly show charge density change with adsorption occurring. All three gases are used as electronic acceptor in the system. CDD makes known ReS_2 becomes polarized and experiences attractive interactions with three gas molecules due to electrostatic forces. CDD comparison of the three, CO and CO_2 show large regions than H_2. The phenomenon just shows that there are greater electrostatic interactions between the two carbon oxides and ReS_2, which also corresponds to the result of

adsorption energy. H_2 shows smallest polarization, its adsorption has smallest electrostatic interaction, the small adsorption energy of H_2 also support this point.

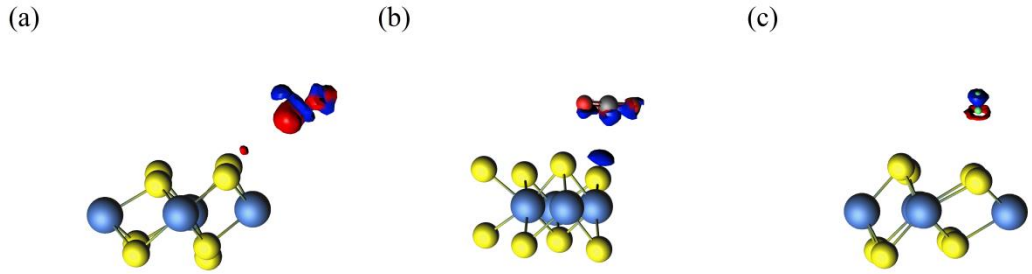

Figure 4.3. CDD of (a) CO, (b) CO_2, (c) H_2**.** The blue distribution corresponds to electrons accumulation, and red distribution corresponds to electrons depletion. The isosurface is taken as 0.0003 a.u. for (c); 0.0005 a.u. for (a), (b).

4.4.4 Density of state (DOS) and Band structure

Gas adsorption may significantly change the electronic properties of adsorbent materials. To better understand how gas adsorption affects the electronic properties of adsorbent materials, we can compare the band structure and DOS of ReS_2 monolayer with those of the adsorption system. **Figure 4.4** presents the band structure of ReS_2 monolayer and the adsorption system, while **Figure 4.5** shows their respective DOS.

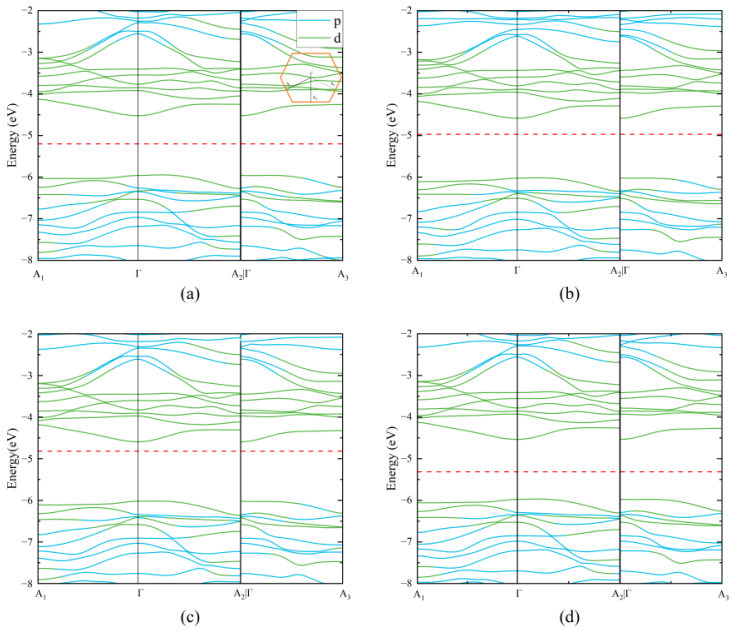

Figure 4.4. Band structure of (a)Pure ReS_2 monolayer, (b)CO-ReS_2, (c)CO_2-ReS_2 and (d)H_2-ReS_2. Fermi levels are shown on this figure as red dotted lines. The Paths of four figure are same.

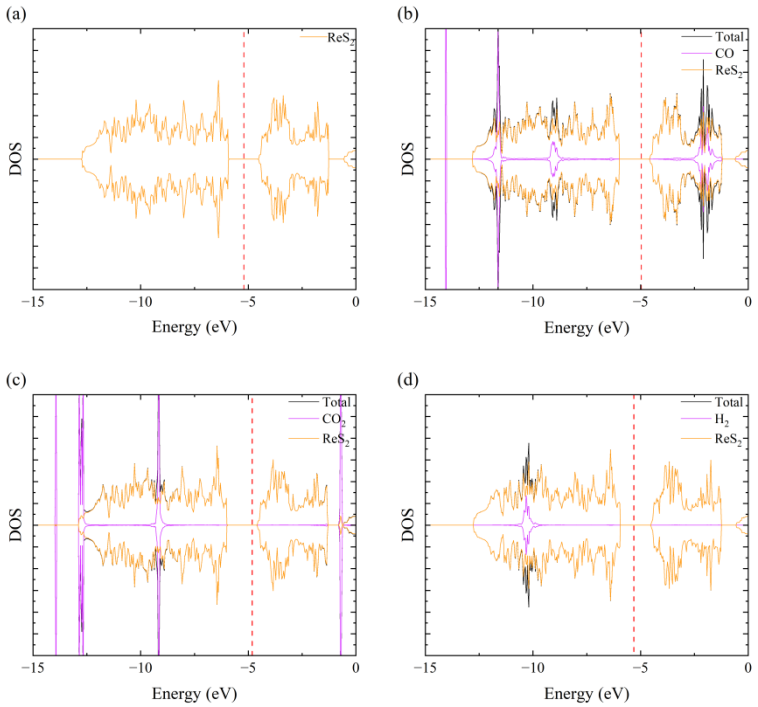

Figure 4.5. DOS of (a)Pure ReS_2 monolayer, (b)CO-ReS_2, (c)CO_2-ReS_2 and (d)H_2-ReS_2**.** Fermi levels are shown on this figure as red dotted lines. 'Total' in DOS means adsorption systems include gas molecule and ReS_2.

The band gap is directly observable and influential properties of a material's electronic structure from band structure and DOS. In the analysis and calculation of ReS_2, we observe that the band gap of pure ReS_2 monolayer is 1.421 eV. In the gas adsorption calculation, CO, CO_2 and H_2 adsorption system on ReS_2 show band gap of 1.432 eV, 1.424 eV and 1.428 eV, respectively. These results indicate a slight enlargement of the band gap in the presence of CO, CO_2 and H_2 adsorption. Thus, the conductivity of ReS_2 has hardly changed without output electrical signal changes when ReS_2 as gas-sensing element. In summary, ReS_2 is not sensitive to these three gases.

In the band structure and DOS, the adsorption of these gases had no impact on the VB and CB. The total adsorption system and ReS_2 states line are nearly coincident in the DOS figures, indicating that the gas adsorption did not significantly alter the electronic structure of ReS_2.

In the band structure, the spin down and spin up energy bands for the three adsorption systems are coincident, indicating that they are nonmagnetic. While the band structure calculates the energy band structure of both spin down and spin up orbits, in this case, they coincided, and thus only the spin-up orbit band structures are shown in the figures. Furthermore, the minimal-energy state in the conduction band and the maximal-energy state in the valence band of the adsorption systems are at the same K point (Γ) in the Brillouin zone. This indicates that the adsorption of the three

gases did not alter the direct band gap of the material. In summary, the adsorption systems have semiconductor properties with nonmagnetic direct band gap like pure ReS_2 monolayer. Although the band gap does not change much, the effect of Fermi level is clearly visible. First, absolute value of Fermi energy represents the work function, and gas adsorption really changed the work function of ReS_2. The work function of CO-ReS_2, CO_2-ReS_2 and H_2-ReS_2 are 4.97 eV, 4.82 eV and 5.31 eV, respectively.

In **Figures 4.4 (b) and (c)**, the Fermi levels are found to be closer to the conduction band than that in **Figure 4.4 (a)**. While the Fermi level of the ReS_2 monolayer was in the middle of the band gap, for CO-ReS_2 and CO_2-ReS_2 systems, the Fermi levels are located closer to the conduction band but did not touch it. Notably, in the CO_2 adsorption system, the CDD analysis revealed that the surface of ReS_2 was an electron-rich region, resulting in a high concentration of electrons that acted as carriers and pushed the Fermi level towards the conduction band.

The study can further analyse the energy band structure according to the DOS. The DOS and the band structure are related concepts in that the density of states is derived from the band structure. The DOS gives information about the number of available states at each energy level. Gas molecules electronic levels mainly distribute in the VB and CB region. In the figure, three kinds of gas adsorptions all show electronic levels contribution in the -10eV. In addition, three gas molecules contribute to the electron band at different energy levels.

Compared to CO and CO_2, H_2 has minimal impact on ReS_2 material. CO and CO_2 adsorption have a higher level of orbital hybridization than H_2 adsorption. Besides, CO and CO_2 contribute to band structure in the CB region that is near to the CBM. However, they do affect the ReS_2 monolayer, without noticeable obvious electronic property change. Three gas molecules' adsorption shows a very low level of orbital hybridization and orbital interaction between the gas molecule and the ReS_2 monolayer.

4.4.5 Effect of extra electric field

The affinity of ReS_2 for the adsorption of the three gases is relatively weak. However, the use of an external electric field can be an effective method for modifying the gas adsorption properties of 2-D materials. Moreover, the application of an electric field is easily implemented and adjusted in the gas adsorption process, making it a promising approach for developing gas sensors based on ReS_2.[129, 146] In this thesis, the molecules CO and CO_2 have lower adsorption energies and absolute charge transfer during adsorption. Therefore, an electric field is employed to improve the adsorption properties of CO and CO_2. In the adsorption configuration image (**Figure 4.2**), the molecule is positioned above ReS_2, while the newly applied electric field opposes this orientation by directing downwards and perpendicularly to the surface of ReS_2. The ±1 V/Å are determined as the electric field range during the gas

configuration optimization and analysis. Due to the extra electric field, the adsorption configuration is altered. The distance of the nearest atom between the gas molecule and the ReS_2 monolayer is the most obvious and direct. Change of distance means the adsorption configuration and, consequently, the adsorption properties are affected. Among all adsorption properties, adsorption energy and charge transfer have the most impact on gas sensitivity. Under the condition of an external electric field, the distances between the nearest atoms, adsorption energies, and charge transfers for the gas-adsorbed ReS_2 monolayer are presented in **Tables 4.8** and **4.9**. In addition, the data are plotted as a broken line graph in **Figure 4.6** to intuitively observe the changing trend with the extra electric field.

Figure 4.6 indicates that the electronic properties are indeed correlated to the intensity of electric field. An ±1 V/Å electric field has little effects on the adsorption energy and charge transfer, while $|E_a|$ and $|Q|$ are greatly affected. However, there is little change in the adsorption configuration due to the presense of a ±1 V/Å electric field. Therefore, a higher electric field can be applied to characterise the effect of the applied electric field in **Figure 4.7**. To significantly enhance adsorption properties, the electric field intensity must exceed $|4|$ V/Å.

Table 4.8 Adsorption properties of CO with application of electric field: (1) Extra electric field strength, (2) Nearest atoms between gas and ReS_2, (3) Distance(D) between nearest atoms, (4) Adsorption energy and (5) charge transfer. Negative value represents charge from gas to ReS_2. Positive means charge from ReS_2 to gas.

Electric field(V/Å)	Nearest atoms	Distance(Å)	Adsorption energy(eV)	Charge transfer(eV)
-1	O-S	3.097	-0.260	0.0270
-0.8	O-S	3.091	-0.256	0.0174
-0.6	O-S	3.088	-0.255	0.0068
-0.4	O-S	3.082	-0.256	-0.0031
-0.2	O-S	3.075	-0.259	-0.0109
0	O-S	3.076	-0.264	-0.0207
0.2	O-S	3.062	-0.262	-0.0327
0.4	O-S	3.040	-0.271	-0.0429
0.6	O-S	3.000	-0.277	-0.0569
0.8	O-S	2.961	-0.285	-0.0717
1	O-S	2.937	-0.306	-0.0884

Table 4.9 Adsorption properties of CO_2 with application of electric field: (1) Extra electric field strength, (2) Nearest atoms between gas and ReS_2, (3) Distance(D) between nearest atoms, (4) Adsorption energy and (5) charge transfer. Negative value represents charge from gas to ReS_2. Positive means charge from ReS_2 to gas.

Electric field(V/Å)	Nearest atoms	Distance(Å)	Adsorption energy(eV)	Charge transfer(e)
-1	C-S	3.182	-0.285	0.0093
-0.8	C-S	3.171	-0.285	0.0021
-0.6	C-S	3.163	-0.286	-0.0049
-0.4	C-S	3.153	-0.288	-0.0118
-0.2	C-S	3.147	-0.29	-0.0186
0	C-S	3.136	-0.293	-0.0262
0.2	C-S	3.125	-0.297	-0.033
0.4	C-S	3.113	-0.302	-0.0407
0.6	C-S	3.097	-0.309	-0.0491
0.8	C-S	3.074	-0.318	-0.0586
1	C-S	3.053	-0.329	-0.0695

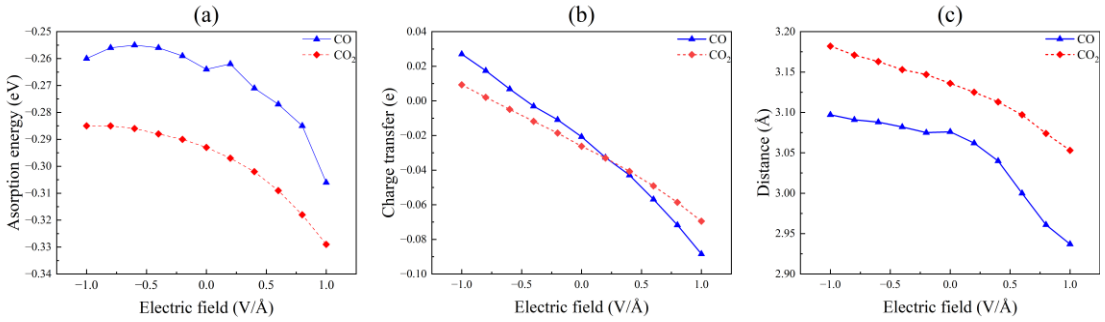

Figure 4.6. Adsorption energy and charge transfer as a function of applied external electric field. Negative charge transfer still indicates that the charge is transferred from the gas molecule to ReS_2.

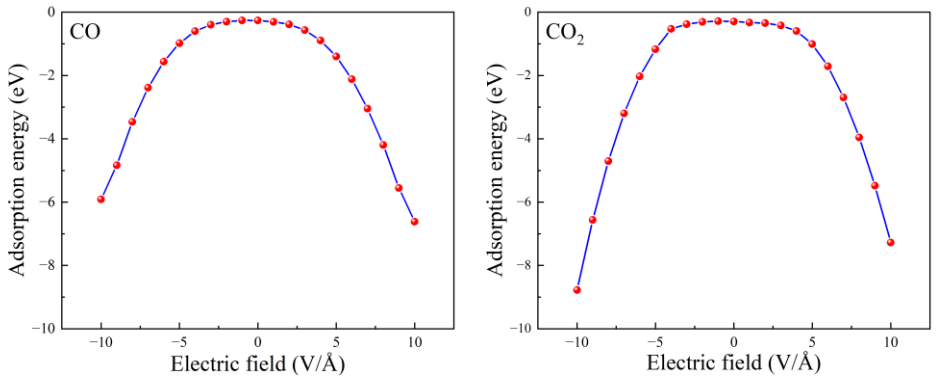

Figure 4.7. Adsorption energy as a function of applied larger external electric field.

4.5 Conclusion

In this chapter, the adsorption properties and configurations of CO, CO_2, and H_2 on a monolayer of ReS_2 are analysed using first-principles calculations. The results show that the adsorption energy of all three gases is negative, indicating that the adsorption process is spontaneous and results in a decrease in the total energy of the system. The most stable adsorption site is determined to be in the middle of the region between the two Re chains. CO_2 has the most stable adsorption configuration with an adsorption energy of 0.293 eV, while H_2 has the most unstable adsorption configuration with an adsorption energy of -0.071 eV. The adsorption energy of CO on a monolayer of ReS_2 is -0.207 eV. Thus, the calculated adsorption energies suggest that CO and CO_2 exhibit stable configuration on the ReS_2 monolayer, while H_2 is less so.

CDD proves that there is a weak interaction between the three gas molecules and the ReS_2 surface. CO and CO_2 systems have far stronger interaction far than the H_2 system. Furthermore, the low flow of charge transfer in the adsorption systems was all found to occur from the gas molecules to the ReS_2 monolayer. All gas molecules are electrons acceptors. Gas molecules adsorption only depends on Van der Waals force.

The electronic structure results of the study indicate that the adsorption of CO, CO_2, and H_2 on the ReS_2 monolayer almost do not influence its semiconductor properties. The band gaps of the ReS_2, CO-ReS_2, CO_2-ReS_2, and H_2-ReS_2 systems were found to be 1.421 eV, 1.432 eV, 1.424 eV, and 1.428 eV, respectively. The gas adsorption caused only a slight increase in the band gap, resulting in a slight increase in the resistance of the ReS_2 layer. The electronic levels are primarily distributed in the VB and CB regions, which are located far from the VBM and CBM. Almost constant electronic structures properties indicate that there is little orbital impurity between them and conductivity of the material almost does not change. In summary, the interaction between ReS_2 and the three gases is minimal, and there is only a slight change in electronic properties. This indicates that ReS_2 may not be highly suitable as a gas-sensing material for these gases.

An additional electric field was applied to optimise the adsorption configuration, but the results show that the effect on the adsorption energy ($|E_a|$) and charge transfer ($|Q|$) is not significant within the scope of ±1 V/Å. Therefore, ReS_2 is not a suitable material for gas sensing of CO, CO_2, and H_2. If future application and study really want to strengthen the adsorption properties of ReS_2 to these gases, the modification of ReS_2 materials, including defect functionalization, heterojunctions and doping, must be considered.

Chapter 5

Optimisation and analysis of NO_2 and NO adsorption configuration on ReS_2

5.1 Synopsis

Chapter 4 presents calculations of the adsorption configuration and properties of CO, CO_2, and H_2 on ReS_2, which have not been previously studied for adsorption on this material. In this chapter, nitrogen oxides is studied. NO_2 has been proved extremely high adsorption sensitivity on the ReS_2 layer. Therefore, the adsorption properties of nitrogen oxides such as NO and NO_2 on the ReS_2 surface are crucial and will be investigated in this chapter. Our calculations on NO_2 can be compared to previous studies to further analyse the interaction between the gas molecule and the 2-D material. NO and NO_2 are both free radical nitrogen oxides; thus, it is also expected that NO will exhibit excellent adsorption properties on the ReS_2 surface.

5.2 Introduction

Anthropogenic nitrogen oxides in the atmosphere come from combustion for thermal power, traffic exhaust, and metallurgical industrial waste. NO_2 and NO are the most hazardous nitrogen oxides.

NO_2, the most prevalent form of nitrogen oxides, is a major air pollutant gas and an important feedstock for the chemical industry. It is a reddish-brown gas above 70°F, and a colourless to brown liquid at room temperature. NO_2 large-scale emission in the atmosphere will affect the formation of secondary fine particles and tropospheric ozone. NO_2 also play an essential role in human safety and health. NO_2 cause serious adverse effects on humans, such as chronic respiratory diseases, eczema and otitis media. Meanwhile, it affects the term mortality of the lung-heart disease, depression and changes in blood lipid levels.[147, 148] NO_2 will also form nitric acid with moisture under wet conditions which may corrode the machine or cause bodily injury. The NO_2 OSHA PEL (permissible exposure limit) is only 5 ppm (Ceiling). The concentration of NO_2 should be effectively monitored to protect the health of humans and the

environment.

NO is a colourless nitrogen oxide that is toxic to the environment. It, along with NO_2, is a major nitrogen oxide produced by combustion sources and is considered a harmful pollutant. At the same time, it is highly toxic, like NO_2. OSHA PEL (8-h TWA) of NO is 25 ppm that data from the U.S. DEPARTMENT OF LABOR. 25 ppm NO short-touch would cause death, and even lower than this concentration will cause pulmonary edema and asthma. Even if not inhaled, NO vapour can irritate eyes. Leakage of high concentration can result in an ashore and violent explosion. Besides its hazard, NO can be a medication in medicine and biology with low optimal concentrations. It is synthesised by Nitric oxide synthases (NOSs) and has complex function action in the human body,[149] for example, it can be a neurotransmitter, a signal influencing biological processes and even a part of the human immune response.[150] Meanwhile, NO is easily oxidized to NO_2, which can cause other serious results.

Furthermore, while excessive levels of NO can have negative effects on health, it's important to note that exogenous NO inhalation therapy is also commonly used to treat pulmonary hypertension in both children and adults.[151] In summary, while NO can have positive effects on physiological functions in appropriate low concentrations for medical applications, it can also cause disease in high concentrations. As a result, it is essential to monitor NO levels in real-time with high sensitivity, both in situations such as daily life and industrial production where exposure to high levels of NO may occur, as well as in medical applications. Highly sensitive monitoring of NO can aid in protecting human health and preventing negative health effects associated with excessive NO exposure.[152]

The objective of this chapter is to determine the most stable configuration of NO_2 and NO on the ReS_2 monolayer and analyse their adsorption properties using first principles calculations. Unlike the three gases studied in the previous chapter, NO_2 and NO are stable odd electron molecules with a total number of valence electrons that is an odd number. The adsorption configurations of NO_2 and NO on ReS_2 will also be investigated and analysed in this chapter.

These molecules with odd electrons are referred to as free radicals. Within the nitrogen oxides group, only NO and NO_2 are classified as free radical molecules. NO is a heteronuclear diatomic molecule and a stable free radical that violates the octet rule. It contains 11 valence electrons, with 5 from the nitrogen (N) atom and 6 from the oxygen (O) atoms. Due to N's lower electronegativity than O, the unpaired α electron is located on the N atom, and 60% of spin density is concentrated there when the neutral NO molecule is formed, making the N atom more prone to react and bond.[153] In contrast, the Lewis structure of NO_2 contains a total of 17 valence electrons, with O atoms possessing a lower electronegativity.

They introduce questions about non-closed shell systems for the theoretical calculation. NO and NO_2 both may change the electronic properties of 2-D materials after adsorption due to an extra electron in a gas molecule. In MoS_2 adsorption

calculation, NO and NO_2 significantly changes the band structure of the 2-D MoS_2.[154] ReS_2 band structure and DOS is also affected by NO_2 in the adsorption calculation.[89] Meanwhile, ReS_2 showed high NO_2 sensitivity. Thus, we are more curious about the role of NO and NO_2 in this chapter.

5.3 Simulation Details

The computational procedures and initial configurations with five active sites are same as in chapter 4. However, NO_2 and NO are very different from CO, CO_2 and H_2. They have a free unpaired electron. Thus, unrestricted calculations must be checked for spin down and spin up in these calculations. In the NO and NO_2 adsorption, open shell gas molecules adsorption properties will be greatly affected by separate calculation of up and down orbits. The calculation process is the same as the first three gases calculations.

5.4 Result and Discussion

5.4.1 Most stable configuration

Table 5.1 presents the adsorption energy data for the initial configurations of the NO_2 and NO adsorption systems, which are listed separately in **Table 5.1** and **Table 5.2**, respectively. All adsorption energy values in the table are negative, indicating that energy is released during the NO and NO_2 adsorption processes, thereby confirming that the adsorption of these gas molecules is spontaneous and exothermic. LDA results only provide an unlimited range of absolute values for adsorption energy, subsequent adsorption properties were also calculated using the PBE-D4 method.

Table 5.1 Adsorption energy of NO_2 adsorption configuration.

		Adsorption energy(eV)	
Active site	Initial configuration	LDA	PBE-D4
P1	Parallel	-0.72	-0.512
	Perpendicular	-0.707	-0.499
P2	Parallel	-0.708	-0.489
	Perpendicular	-0.717	-0.512
P3	Parallel	-0.702	-0.48
	Perpendicular	-0.701	-0.48
P4	Parallel	-0.703	-0.48
	Perpendicular	-0.719	-0.503
P5	Parallel	-0.707	-0.484
	Perpendicular	-0.718	-0.503

Table 5.2 Adsorption energy of NO adsorption configuration.

		Adsorption energy(eV)	
Active site	Initial configuration	LDA	PBE-D4
P1	Parallel	-0.39	-0.13
	O atom above N atom	-0.554	-0.415
	N atom above O atom	-0.693	-0.415
P2	Parallel	-0.668	-0.434
	O atom above N atom	-0.573	-0.39
	N atom above O atom	-0.704	-0.405
P3	Parallel	-0.669	-0.421
	O atom above N atom	-0.452	-0.414
	N atom above O atom	-0.703	-0.405
P4	Parallel	-0.718	-0.417
	O atom above N atom	-0.559	-0.331
	N atom above O atom	-0.681	-0.323
P5	Parallel	-0.643	-0.421
	O atom above N atom	-0.573	-0.389
	N atom above O atom	-0.485	-0.415

To select the most stable adsorption configurations, it is necessary to compare the absolute values of adsorption energies. The adsorption configuration with the most negative energy release is considered the most stable one. In the NO_2 adsorption table, there are two identical results, so it is important to compare whether the configurations of these two results are the same. Since the adsorption configurations with the same maximum adsorption energy in the NO_2 adsorption table are identical, they can be considered as a single configuration. The data of the most stable configurations are summarised in **Table 5.3** and pictures of configurations are also showed in **Figure 5.1**. In the **Table 5.3**, 'nearest atoms' and 'distance' are from PBE-D4 result, and configuration pictures also. Here, 'nearest atoms' means the nearest atoms between gas molecules and ReS_2.

The value of adsorption energy directly reflects the adsorption strength. NO and NO_2 adsorption systems show far greater adsorption energy absolute value than CO, CO_2 and H_2 systems. In the last chapter, CO_2 has the largest energy release (0.294 eV), which less than either NO or NO_2 systems.

The adsorption energy for the NO system was found to be -0.434 eV, while the largest adsorption energy was observed for NO_2 (-0.512 eV). Moreover, it has been experimentally and computationally confirmed that NO_2 is a highly sensitive gas for adsorption on ReS_2. In a previous study, the adsorption experiment confirmed the high selectivity of ReS_2 for NO_2, and subsequent calculations were performed to provide a more detailed analysis of the adsorption properties.[4, 89]

Table 5.3 Adsorption properties of NO_2 and NO most stable adsorption configuration. (1) Adsorption energy calculated by LDA and PBE-D4 XC function. The negative energy means energy is released in adsorption. (2) Nearest atoms between gas and ReS_2 and (3) Distance(D) between nearest atoms.

Gas	Adsorption energy (eV)		Nearest atoms	D(Å)
	LDA	PBE - D4		
NO_2	-0.72	-0.512	O-S	2.746
NO	-0.718	-0.434	N-S	2.23

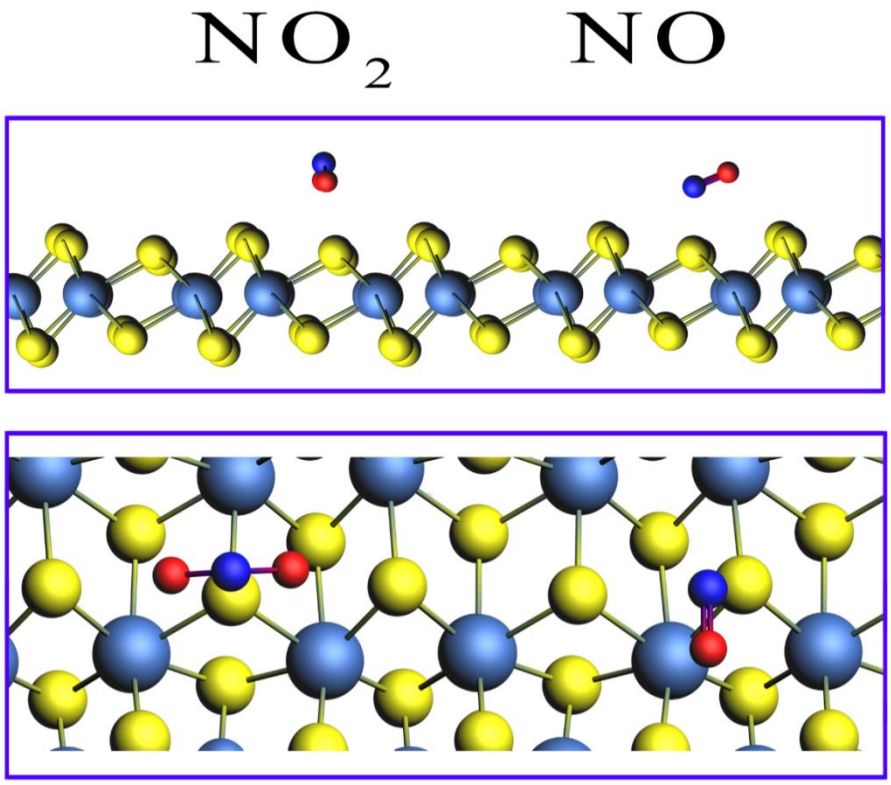

Figure 5.1. Top view and side view of NO_2 and NO adsorption system. The direction shown in the side view is consistent with the extension direction of Re chain. The top view shows the region between the two Re chains. In the gas molecule, green atom is hydrogen, red atom is oxygen and dark blue atom is nitrogen.

The adsorption configuration of NO_2 in our work agrees with other recent studies. However, it is important to note that we should consider the treatment of up and down spin orbitals for free radical calculations, i.e., unrestricted calculations. These effects were omitted in the literature.[89] Free radical calculations require the independent

treatment of up and down spin orbitals, as the presence of an unpaired electron in a free radical makes it spin-dependent. In this study, the adsorption energy without orbits independent calculation was also calculated for a comparison. The result of NO_2 adsorption is -0.745 eV, which is greater than data from Zhou's work and **Table 5.3**.[89] A substantial formation energy observed during NO_2 adsorption on the ReS_2 surface, akin to the findings of the previous study,[89] implies the stability of the adsorption system and a pronounced level of interaction between the species.

NO in the calculation shows only below and close to NO_2 adsorption energy. It means NO-ReS_2 adsorption configuration is also very stable and, ReS_2 has a promising potential for NO highly selective sensing. The nearest atoms of NO_2 and NO molecules to S atoms of the ReS_2 surface are O and N atoms. In fact, two O atoms in the NO_2 molecule have almost the same distance to an S atom. O and N atoms are low electronegativity atoms in the NO_2 and NO gas molecules. The distance between two kinds of monoxide and S atom in the ReS_2 monolayer are shorter than those reported in the previous chapter results. H_2 shows shortest distance between nearest atoms in the previous chapter, which is 3.006 Å. On the contrary, NO_2 and NO adsorption systems show shorter distance, which are 2.746 and 2.23 Å, respectively. The short distance is directly related to the large amount of energy released during the adsorption process.

5.4.2 Charge transfer

Stable adsorption configuration is only one of the adsorption properties to be analysed. Charge transfer is also a very important property for adsorption analysis. The atomic charge transfer values of NO_2 and NO are shown in **Table 5.4** and **Table 5.5**. Same as the previous chapter, results from multiple charge analysis methods would be exhibited.

Table 5.4 Charge transfer in NO_2 adsorption configuration. Negative value represents charge from gas molecule to ReS_2. Positive means charge from ReS_2 to gas molecule.

Methods for Charge	Single gas molecule (e)			Gas in adsoprtion system (e)			Transfer(e)
	N	O	O	N	O	O	
Hirshfeld	0.167	-0.084	-0.083	0.127	-0.102	-0.102	-0.077
VDD	0.196	-0.098	-0.097	0.159	-0.097	-0.096	-0.035
CM5	0.076	-0.038	-0.038	0.032	-0.061	-0.06	-0.089
Mulliken	0.493	-0.247	-0.246	0.441	-0.277	-0.276	-0.112

Table 5.5 Charge transfer in NO adsorption configuration. Negative value represents charge from gas molecule to ReS_2. Positive means charge from ReS_2 to gas molecule.

Methods for Charge	Single gas molecule (e)		Gas in adsoprtion system (e)		Transfer(e)
	N	O	N	O	
Hirshfeld	0.021	-0.021	0.003	-0.051	-0.048
VDD	0.029	-0.029	0.031	-0.04	-0.009
CM5	-0.031	0.031	-0.071	-0.002	-0.073
Mulliken	0.167	-0.167	0.097	-0.192	-0.095

Charge transfer of NO_2 and NO is more significant than that of CO, CO_2 and H_2 adsorption. NO_2 shows -0.077 e charge transfer and NO shows -0.048 e charge transfer by Hirshfeld charge analysis. Thus, ReS_2 surface may be sensitive to NO_2 and NO.

CM5 analysis provides further charge analysis of single gas molecules compared to those obtained from Hirshfeld. Therefore, their charge transfer results are also different. CM5 method charge transfer results of NO_2 and NO are -0.089 e and -0.073 e, respectively. VDD approach also gives a similar charge analysis pattern to the Hirshfeld technique. In summary, the charge transfer in NO_2-system is greater than NO-system, and both are greater than the charge transfer of the three gases in the previous chapter. Large charge transfer may cause change of ReS_2's electronic structure, more accurate information needs to be provided by band structure and DOS.

5.4.3 Charge density difference (CDD)

Adsorption energy can indicate great interaction between the two nitrogen oxides and the ReS_2 monolayer. Now, a more intuitive way to analyse the interaction is necessary.

This difference in electron density can result from the transfer of electrons from one region to another, creating an excess of electrons in one region and a deficit in the other. CDD of NO_2 and NO systems are shown in **Figure 5.2**.

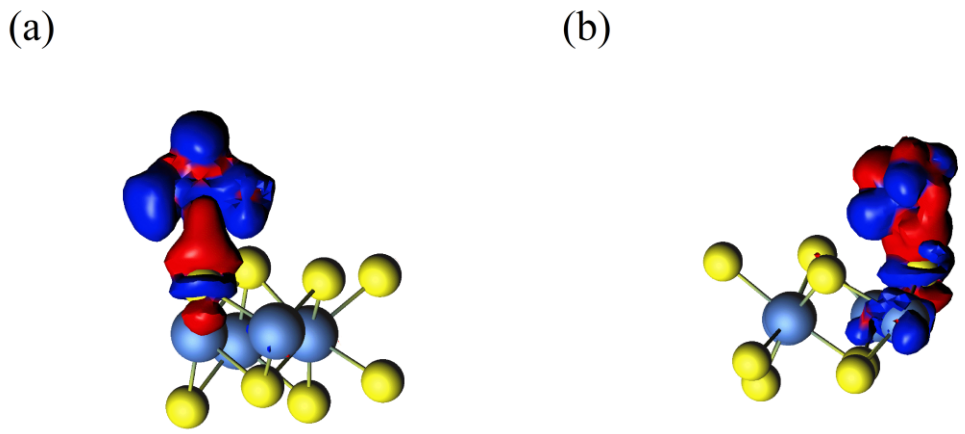

Figure 5.2. CDD of (a)NO_2 and (b)NO adsorption configurations. The blue distribution corresponds to electrons accumulation, and red distribution corresponds to electrons depletion. The iso-surface is taken as 0.0005 a.u. for (a), (b).

Figure 5.2 shows that the charge density difference region of NO_2 and NO are significantly larger than CO, CO_2 and H_2. A larger charge density difference region in adsorption suggests a stronger interaction between gas molecules and ReS_2 and indicates a significant transfer of electrons from the adsorbate to the adsorbent, resulting in a higher degree of electron localization in the adsorbent. Meanwhile, electron transfer is also driven by the desire to minimize the overall energy of the system. Thus, maximum electrostatic force and charge transfer indicated by density difference explain why the adsorption energy (formation energy) of NO_2 and NO systems (-0.512 eV and -0.434 eV) are larger than CO, CO_2 and H_2 (-0.264 eV, -0.293 eV and -0.071 eV).

The most noteworthy is the excellent interaction and form of interaction between the two gases and ReS_2. The red region located above the S atom and the blue region surrounding the NO_2 molecule both indicates a significant transfer of electrons from the ReS_2 monolayer to NO_2. **Figure 5.2** illustrates that the electron depletion region is situated between the NO and the S atom, and it simultaneously interacts with both of them. During the adsorption process, electrons flow to both the gas molecule and the material simultaneously, which can restrict charge transfer and interaction between NO and ReS_2. The preceding assertion finds support in the tabulated data discussed earlier in the text (**Tables 5.2** and **5.3**), which clearly indicates that the adsorption energy and charge transfer associated with NO adsorption are both lower compared to those of NO_2 adsorption.

5.4.4 Density of state (DOS) and Band structure

The adsorption of a molecule on a surface can be influenced by the presence of specific orbital levels or energy states in the molecule that can interact with the surface. Understanding the band structure and DOS of both the surface and the adsorbate can therefore provide crucial information for accurately predicting the adsorption behaviour of materials. It is possible that the extra electron in NO_2 and NO can lead to stronger orbital hybridization during adsorption. **Figures 5.3** and **5.4** include the band structure and DOS of the ReS_2 monolayer and the adsorption systems. The adsorption of the two gases leads to the drastic change of the electronic structure of the ReS_2 surface.

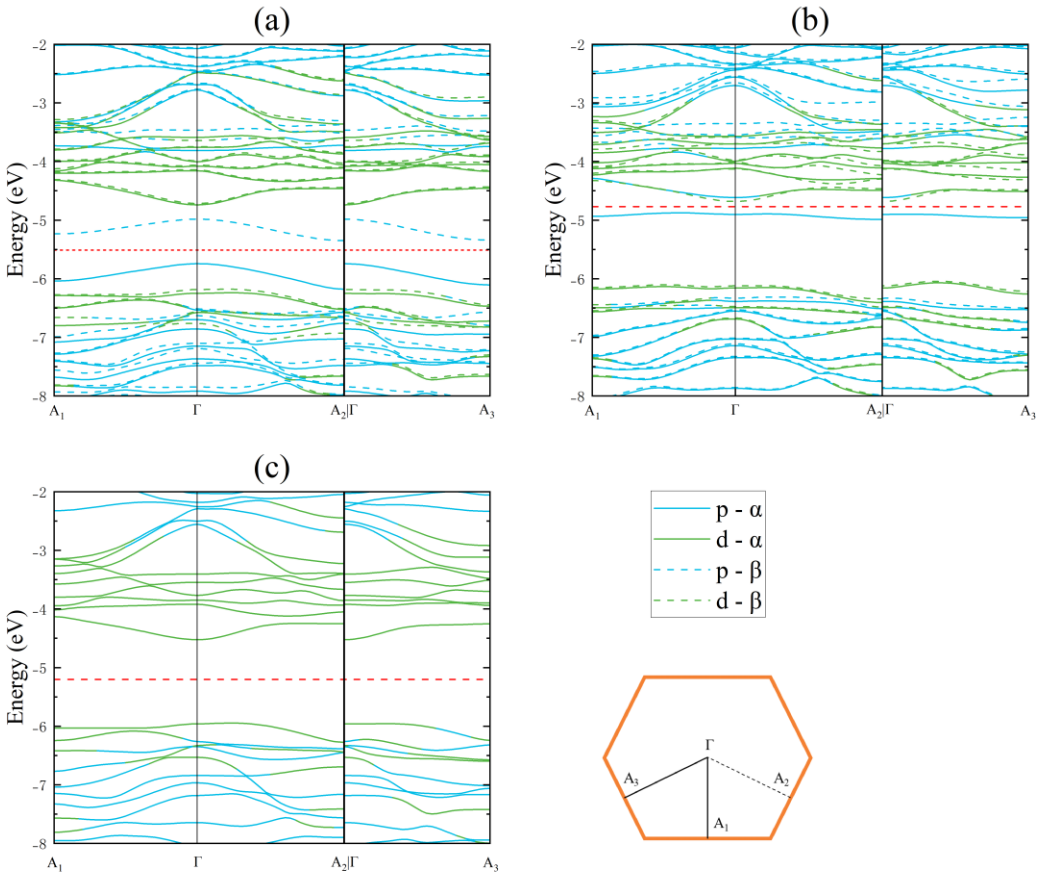

Figure 5.3. Band structure of (a)NO_2-ReS_2, (b)NO-ReS_2, (c)Pure ReS_2 monolayer. Fermi levels are shown on this figure as red dotted lines. The path of band structure analysis is (A_1 – Γ – $A_2|A_3$). The Spin up and down band no longer coincide in two nitrogen oxide gas adsorption configurations.

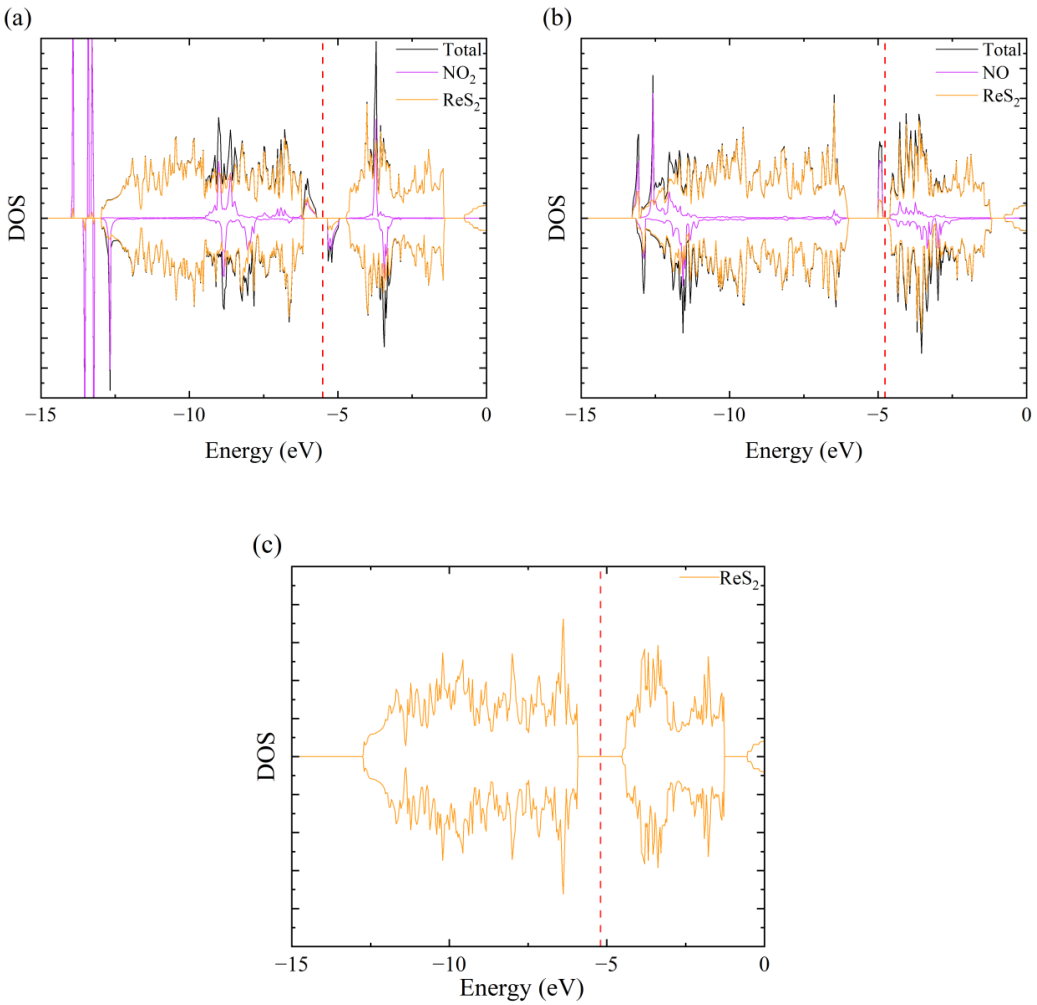

Figure 5.4. DOS of (a)NO_2-ReS_2, (b)NO-ReS_2, (c)Pure ReS_2 monolayer. Fermi levels are shown on this figure as red dotted lines. 'Total' in DOS means adsorption systems include gas molecule and ReS_2.

The spin up and down bands no longer coincide after gas adsorption, indicating that the energy levels of the spin up and down electrons have shifted relative to one another. The shift in the energy levels of the spin up and down electrons could indicate that the material has become magnetic, or that its magnetic properties have changed. Magnetism arises from the alignment of the magnetic moments of electrons in a material. Just right, the electronic properties of ReS_2 have been greatly modified by NO_2 and NO adsorption. Band gaps of NO_2-ReS_2 and NO-ReS_2 are 0.395 eV and 0.195 eV. Fermi level do not pass through bands in their band structures. Fermi energy lines also show the work function of NO_2 and NO systems that are 5.51 eV and 4.77 eV. NO-adsorption still has a direct band gap, NO_2-systems, while NO_2 loses the direct band gap. However, a band gap close to 0 represents an increase in conductivity, resulting in a significant change in electrical signals after gas adsorption.

In the system of NO and NO_2 adsorption, it is possible to observe the manifestation of orbital hybridization in the band structure and DOS plots. Notably, the results

obtained for NO_2 display consistency with prior computational results, although spin up and down orbits are not included in previous study.[89] Upon the adsorption of NO and NO_2 on the ReS_2 surface, new gap states are generated in proximity to the Fermi level by impurity level caused by orbital hybridization. These gap states exhibit a significant impact on the p orbital energy level character of the 2-D material. NO_2 adsorption greatly contributes VBM and CBM energy level at the same time. A comparison between the DOS of the NO_2 system (**Figure 5.4a**) and the ReS_2 monolayer (**Figure 5.5a**) also support this conclusion. Compared with the ReS_2 monolayer, the DOS in the Figure 5.4(c), NO_2 adsorption brings peaks on both sides of the Fermi level. NO pushes fermi energy to the CBM, and introduce new states for the new VBM. The fermi energy will move closer to the conduction band and increase the likelihood of electrons being able to participate in conduction. The minimal energy band gap of the material results in exceptional electrical conductivity, exhibiting characteristics of a semimetal, requiring a minimal amount of energy to facilitate transitions between the valence and conduction bands. Further characterisation is shown in **Figure 5.5** with the PDOS analysis.

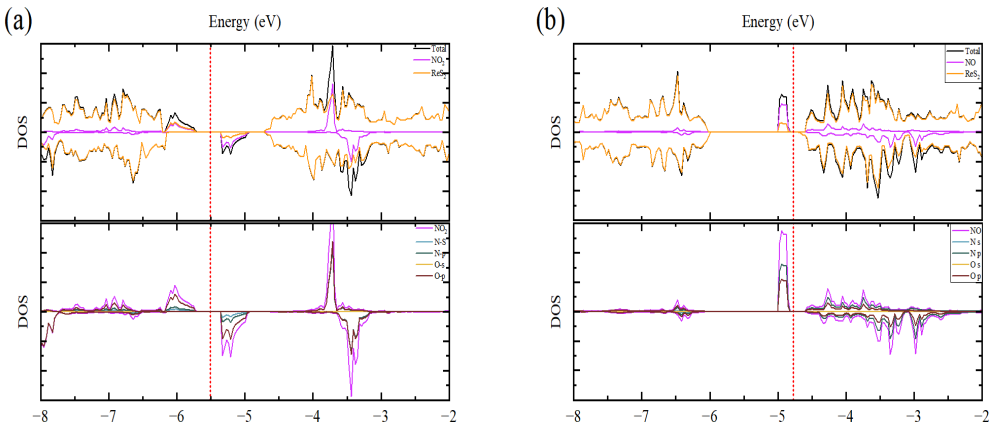

Figure 5.5. PDOS of (a)NO_2 and (b) NO. Fermi levels are shown on this figure as red dotted lines.

In **Figure 5.5 (a)**, O-p make a great contribution to the new states (VBM and CBM) around the Fermi level. The NO_2 adsorption on material introduces new states or bands in the vicinity of the Fermi level, mainly due to the heterozygosity of the p orbitals. The newly introduced VBM band corresponds to the spin-up p orbital, while the CBM band represents the spin-down p orbital. The adsorption of NO also results in the formation of new states or bands for the VBM and CBM, leading to electronic structure rebuilding. In comparison to NO_2, the contribution of the N-p orbital to the system's VBM is more significant and even surpasses that of the O-p orbital. The contribution of these atoms to the state corresponds to nearest atoms in the adsorption configurations of the gases.

In summary, NO and NO_2 absorption leads to the reduction of the band gap, resulting in extremely high conductivity. When ReS_2 is used as gas sensing material in gas sensor, electrical signals will change greatly due to the adsorption of NO_2 and NO. So ReS_2 is extremely sensitive to NO_2 and NO.

5.4.5 Electron localization function (ELF)

It is of significant importance to examine the interaction between NO and NO_2 with a ReS_2 monolayer, given the observed high degree of orbital hybridization and pronounced alterations in the electronic properties of ReS_2 in their presence. Meanwhile, CDD suggests that NO and NO_2 adsorption systems have great interaction between gas molecules and ReS_2 monolayer. Further investigation is required to determine the magnitude and the nature of this interaction. However, whether there is bond formation is a key point.

The electron gas that has been measured was compared to the uniform electron gas, with the ELF serving as a metric of comparison. A value of 0.5 for ELF corresponds to perfect delocalization of electrons and is characterized as a uniform electron gas, while a value of 1 for ELF indicates perfect localization of electrons.[124-126] And, when ELF = 0, it means a low electron density, although ELF is not a value that directly reflects the electron density.[155] The extent of electron localization can provide insight into both lone electron pairs and bonding interactions. In order to deeply analyse the interaction between NO and NO_2 gases and the material, the ELF for these nitrogen oxides is presented in **Figure 5.6**.

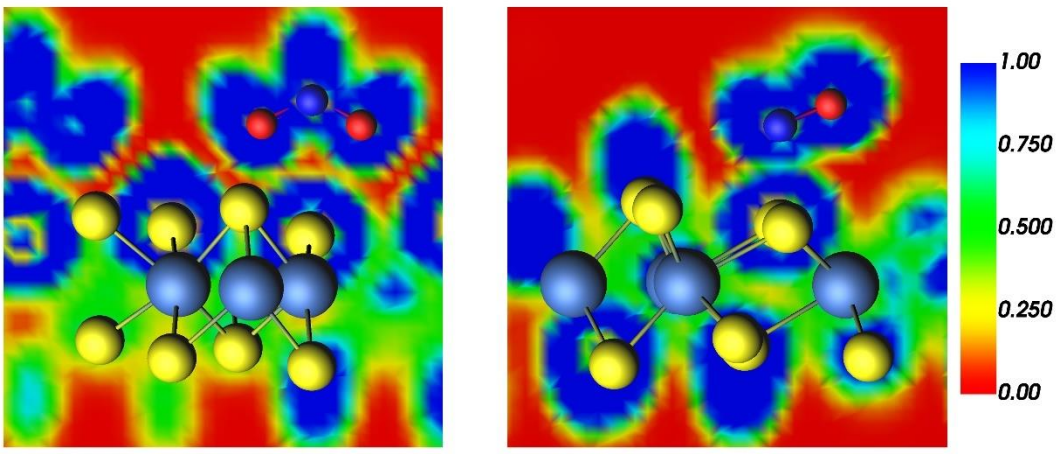

Figure 5.6. ELF of (a)NO_2 and (b)NO.

In **Figure 5.6**, the red area means zero value of ELF, and the blue area means one value of ELF and perfect localization. The region between the O atoms and the S

atom is depicted in yellow, indicating an ELF value less than 0.5 and approaching 0.25. This observation suggests that no new chemical bonds were formed during the adsorption process, thereby inferring that the adsorption of NO_2 onto ReS_2 is not a chemical adsorption process. The ELF value, despite not being equal to zero, merely signifies a high degree of orbital hybridization between the molecules and ReS_2. Thus, despite the large substantial interaction between NO_2 and the material, a chemical bond does not form. However, the bent structure of NO_2 facilitates more efficient orbital hybridization, resulting in a greater degree of electronic structure modification and interaction.

The conditions determining the adsorption of NO gas molecules in Figure 5.6(b) are diverse in nature. In the NO-ReS_2 system, the S atom in ReS_2 and the N atom in the NO molecule represent the closest atoms. The EFL in the region between these two atoms is estimated to be within the range of 0.5 to 0.75, signifying a moderate level of electron localization and the existence of free electrons. The possibility of the formation of a metallic-like bond during adsorption, along with accompanying metallic properties, cannot be overlooked.[156] The unpaired electron in NO interacts more strongly with the surface orbitals, leading to a greater degree of orbital hybridization and modification of the electronic structure of the surface than NO_2. A more intuitive and data-driven analysis of orbital interactions can be computed using EDA and NOCV.

5.4.6 Energy decomposition analysis - Natural Orbitals for Chemical Valence (EDA - NOCV)

Using the EDA-NOCV method, it is possible to accurately capture the complex interactions between the gas and the material and quantify the energetics of gas adsorption in ReS_2. EDA-NOCV could be a further energy analysis method for orbital interactions. This is essentially the contribution of complementary orbital pairs to the total orbital interaction energy (ΔE_{oi}), which takes into account several key factors, including orbital mixing, relaxation, charge transfer, and polarization. The NOCV method can provide a more accurate representation of the electronic structure of the adsorption system, resulting in a more thorough understanding of orbital interactions between the gas molecule and the ReS_2 surface and their impact on the adsorption process.

The adsorption energy of NO_2 and NO are -0.512 eV and -0.434 eV, respectively. The orbital action energy needs to be decomposed from the adsorption energy firstly by EDA. Adsorption energy includes electrostatics energy (ΔE_{elstat}), Pauli repulsion (ΔE_{Pauli}), orbital interactions (ΔE_{oi}) and dispersion energy (ΔE_{disp}). According to calculation of EDA, contribution of each term could be separated from total energy. In addition, NOCV only analyses orbital interactions (ΔE_{oi}): 1) in NO_2-ReS_2 system, ΔE_{oi} = -75kJ/mol. 2) in NO-ReS_2, ΔE_{oi} = -207.6 kJ/mol. The orbital interaction

between NO and the ReS_2 surface is much higher than that between NO_2 and the ReS_2 surface. This highlights the fact that the orbital interaction between NO and the ReS_2 surface is much stronger. However, it's important to note that the orbits interaction between NO and ReS_2 surface also leads to greater Pauli repulsion, which can reduce the stability of the adsorption and the whole adsorption process. CDD and adsorption confirmed this point. The entire interaction between the NO_2 system is larger than that of the NO system.

Figures 5.7 and **5.8** show the corresponding deformation electron densities of the pair which has the largest contribution to the total orbital interaction (k = 1). Due to the calculation of open shell molecules, each pair is divided into α (spin up) and β (spin down) orbit.

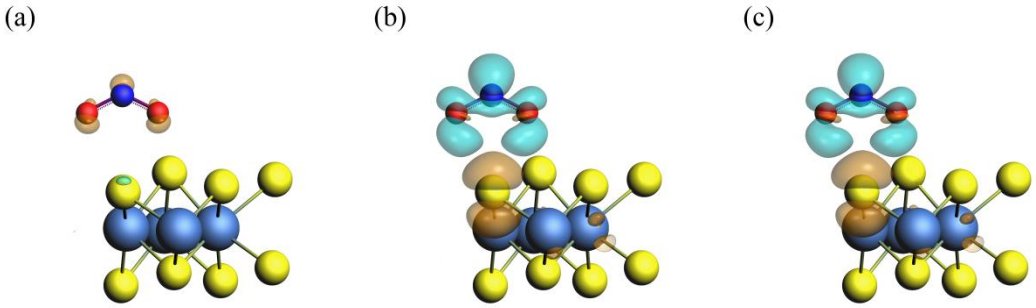

Figure 5.7. Deformation density $\Delta\rho_{(1)}$ that corresponds to ΔE_1 in NO_2-ReS_2 system (a)$\Delta E_{1\alpha} = -9.5\text{kJ/mol}$ (b)$\Delta E_{1\beta} = -39.0\text{kJ/mol}$ (c)$\Delta E_1 = -48.5\text{kJ/mol}$. The electrons flow from the origin region to the blue region. The isosurface is taken as 0.0003 a.u.

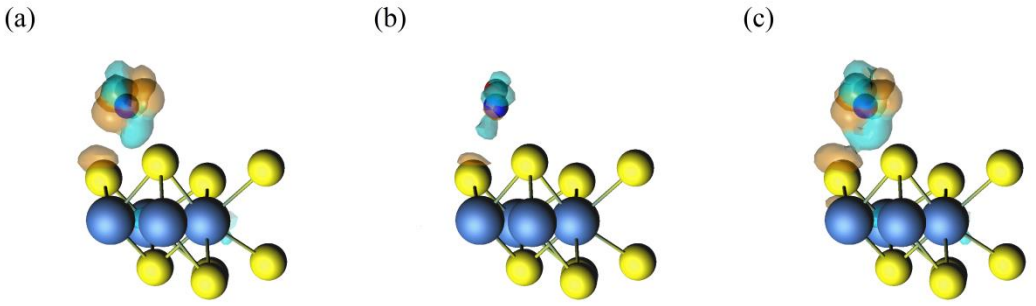

Figure 5.8. Deformation density $\Delta\rho_{(1)}$ that correspond to ΔE_1 in NO-ReS_2 system **(a)** $\Delta E_{1\alpha} = -70\text{kJ/mol}$ (b)$\Delta E_{1\beta} = -60.6\text{kJ/mol}(c)\Delta E_1 = -130.6\text{kJ/mol}$. The isosurface is taken as 0.003 a.u.

The electrons flow from the origin region to the blue region in figures, which blue distribution corresponds to electrons accumulation, and red distribution corresponds to electrons depletion. They contribute most to the orbital energy. **Figure 5.7** shows electrons flow mainly from the ReS_2 surface to the gas molecule (NO_2), although

Figure 5.7 (a) proves that electrons also flow from NO_2 to the ReS_2 surface. Electrons from ReS_2 also confirmed the charge transfer from NO_2 to ReS_2. The electrons are mainly concentrated on the O atom. By comparison, NO adsorption in the NOCV analysis shows a more complex situation in **Figure 5.8**. The whole electronic flow is mainly from S atom in the ReS_2 surface to the NO molecule by orbital interactions. the isosurface used for the NO system is much larger than that for the NO_2 system; thus, the deformation density of the NO adsorption is much greater than that of the NO_2 adsorption. It can directly indicate that NO adsorption has a greater orbit interaction. Meanwhile, deformation density by the NOCV analysis shows no characteristics of covalent bonds in NO adsorption system

5.5 Conclusion

The ReS_2 surface is more sensitive to NO and NO_2 than CO, CO_2 and H_2. The adsorption energy of NO_2-ReS_2 and NO-ReS_2 adsorption systems are -0.512 eV and -0.434 eV, which are far larger than that of the CO_2-ReS_2 system. On the other hand, the charge transfer in these two systems is also larger. Thus, ReS_2 could support stable and sensitive configurations for NO_2 and NO.

The adsorption of the two forms of nitric oxide significantly modifies the electronic structure of the ReS_2, as evidenced by the changes in the band gaps of the ReS_2, NO_2-ReS_2, and NO-ReS_2 systems. The presence of gas molecules introduces new energy levels near the Fermi level, leading to the creation of new VBM and CBM states. As a result, the adsorption system exhibits characteristics of a semimetal with remarkable electrical conductivity. Large changes in conductivity will lead to changes in electrical signals, which is conducive to gas detection.

The stability of the configuration and alterations in the electronic properties render the interaction between gas molecules and the ReS_2 monolayer. The analysis of the CDD, ELF and the NOCV reveals that both NO and NO_2 exhibit a high degree of orbital hybridization with the ReS_2 monolayer. Notably, a metal-like bond is formed between NO and ReS_2, indicating strong orbit interaction between the two species. To conclude, the ReS_2 monolayer shows great potential as an alternative for gas sensing applications, specifically in the detection of NO and NO_2. However, further experiments and calculations are necessary to confirm the adsorption of NO on ReS_2 and to fully explore its potential as an NO gas sensor.

Chapter 6

Conclusion and Future Work

6.1 Conclusions

This thesis employs a first-principles calculation approach based on Density Functional Theory to assess the feasibility of the ReS_2 monolayer as a 2-D gas-sensing material. The investigated target gases include CO, CO_2, H_2, NO_2, and NO. To ensure a comprehensive evaluation, the optimisation of the ReS_2 monolayer unit cell was performed prior to the optimisation of the adsorption configurations. The most stable adsorption configurations selected from the results obtained from the optimisation of various initial configurations. The ultimate stable adsorption arrangements of all gases are situated within the region bounded by two Re-chains. A comprehensive analysis of the adsorption configuration is required to elucidate the sensitivity of ReS_2 towards gas molecules and the characteristics of the adsorption system. The properties that require determination include the adsorption energy, charge transfer, band structure, density of states, and charge density distribution.

Chapter 1 provides an overview of the background of ReS_2 and highlights its potential as a highly sensitive material for gas detection applications. Chapter 2 introduces the theoretical calculation method of this study. First-principles calculations based on DFT are mentioned, and discusses the adsorption properties as well as the software used for these calculations in this chapter. Chapter 3 is focused on the optimisation process and results of ReS_2, specifically in the context of its use as an adsorbate. The structural optimisation of ReS_2 serves as a crucial step in preparing for subsequent adsorption calculations. Chapters 4 and 5 are the most important sections for presenting the results of adsorption properties.

In chapter 4, according to the results of adsorption and charge transfer analysis, ReS_2 exhibits insensitivity to CO, CO_2, and H_2. Furthermore, the band structure and density of states analysis indicate that the adsorption of these three gas molecules has negligible impact on the electronic properties of ReS_2. The affinity of ReS_2 for the adsorption of the three gases is relatively weak. Therefore, the imposition of an electric field is undertaken to characterize the enhancement of the strength of adsorption. A comparison of the calculated adsorption energy and charge transfer results confirms that the application of an electric field can benefit the adsorption of the three gases in question.

Chapter 5 presents the outcome of the adsorption of NO_2 and NO on a ReS_2 monolayer. It is demonstrated that ReS_2 possesses a robust aptitude for the adsorption of the two nitrogen oxide gases in question. This manifestation is evidenced by the comparatively substantial magnitude of the adsorption energy and charge transfer. The CDD displays a substantial and intricate area of density difference. Thus, the interaction between gas and monolayer is a phenomenon in NO_2 and NO adsorption on ReS_2. Band structure and DOS provides a graphical representation of the electronic structure of gases adsorbed on ReS_2. This representation reveals a significant difference between the NO_2-ReS_2 and NO-ReS_2 adsorption systems and pure ReS_2. NO_2 and NO adsorption introduce new energy levels into the electronic structure, causing a decrease in the band gap. Thus, conductivity of the resulting systems is significantly increased, leading to significant changes in the output electrical signals when NO_2 and NO adsorption[157]. This can prove that ReS_2 is sensitive to these two gases. The alteration of the electronic structure of ReS_2 provides evidence of a significant interaction between two gas molecules and the ReS_2. The ELF and NOCV analysis provide insight into the nature of the interaction between gas molecules and the ReS_2 monolayer. The results obtained from these analyses indicate a high degree of orbital hybridization between the gas molecules and the ReS_2 monolayer. The interaction between NO_2 and ReS_2 has been determined to be weaker in comparison to the interaction between NO and ReS_2. The latter interaction has been found to result in the formation of a metal-like bond between NO and ReS_2. Previous experiments and calculations have deemed ReS_2 to be a material of considerable potential as a gas-sensitive material for the detection of NO_2. The current calculation provides a comprehensive examination and verification of the interaction between NO_2 and ReS_2, offering a deeper understanding of the mechanism of gas sensing in this system.[4] Meanwhile, in this study, ReS_2 has demonstrated potential as a gas sensitive material for the detection of NO. However, further experiments and calculations are necessary to confirm the adsorption of NO on ReS_2 and to fully exploit its potential as an NO gas sensor.

6.2 Future work

(1) Experimental verification

This thesis examines five different kinds of gas adsorption on ReS_2. First principles calculation serves as a methodology for research. But simulation is limited. Thus, the outcomes of computational modelling require validation through empirical testing, particularly concerning the adsorption of NO.

(2) Method for adsorption enhancement

The ability of ReS_2 to exhibit a strong response to CO, CO_2 and H_2 is limited, and even the application of an electric field fails to produce a substantial enhancement. The sensitivity and selectivity of ReS_2 can be further improved through the use of

material modification techniques such as Defect Functionalization, Doping, and the creation of Heterojunctions. Of these methods, the Heterojunctions is particularly effective. Due to vdW interactions between the layers and no surface dangling bonds, ReS_2 could become an important participant in functional heterostructures.[74] The application of external electric fields has shown limited efficacy in enhancing ReS_2 adsorption. However, alternative external stimulation methods may prove to be more effective. One such method that has been explored in previous ReS_2 adsorption experiments is light irradiation, and this method holds potential for future experimentation and computational analysis.[4]

Bibliography: Uncategorized References

1. Morris, A. S., Measurement and instrumentation principles. IOP Publishing: 2001.
2. Colls, J., Clay's library of health and the environment: air pollution. **2002,** (Ed. 2).
3. Aswal, D. K.; Gupta, S. K., *Science and technology of chemiresistor gas sensors*. Nova Publishers: 2007.
4. Zeng, J.; Niu, Y.; Gong, Y.; Wang, Q.; Li, H.; Umar, A.; de Rooij, N. F.; Zhou, G.; Wang, Y. J. A. s., All-dry transferred ReS2 nanosheets for ultrasensitive room-temperature NO2 sensing under visible light illumination. *ACS Sensors* **2020,** *5* (10), 3172-3181.
5. Tongay, S.; Sahin, H.; Ko, C.; Luce, A.; Fan, W.; Liu, K.; Zhou, J.; Huang, Y. S.; Ho, C. H.; Yan, J.; Ogletree, D. F.; Aloni, S.; Ji, J.; Li, S.; Li, J.; Peeters, F. M.; Wu, J., Monolayer behaviour in bulk ReS2 due to electronic and vibrational decoupling. *Nat Commun* **2014,** *5*, 3252.
6. Nazemi, H.; Joseph, A.; Park, J.; Emadi, A., Advanced Micro- and Nano-Gas Sensor Technology: A Review. *Sensors (Basel)* **2019,** *19* (6).
7. Dai, J.; Ogbeide, O.; Macadam, N.; Sun, Q.; Yu, W.; Li, Y.; Su, B.-L.; Hasan, T.; Huang, X.; Huang, W. J. C. S. R., Printed gas sensors. *Chemical Society Reviews* **2020,** *49* (6), 1756-1789.
8. Bogue, R.; Loughlin, C., *Gas sensors*. Emerald Publishing Limited: 2017.
9. Makeenkov, A.; Lapitskiy, I.; Somov, A.; Baranov, A., Flammable gases and vapors of flammable liquids: Monitoring with infrared sensor node. *Sensors and Actuators B: Chemical* **2015,** *209*, 1102-1107.
10. Zhang, D.; Yang, Z.; Li, P.; Pang, M.; Xue, Q., Flexible self-powered high-performance ammonia sensor based on Au-decorated MoSe2 nanoflowers driven by single layer MoS2-flake piezoelectric nanogenerator. *Nano Energy* **2019,** *65*, 103974.
11. Wang, L.; Song, J., Enhanced NH3 sensing properties of carboxyl functionalized carbon nanocoil. *Materials Research Express* **2020,** *7* (7).
12. Lee, E.; VahidMohammadi, A.; Prorok, B. C.; Yoon, Y. S.; Beidaghi, M.; Kim, D. J., Room Temperature Gas Sensing of Two-Dimensional Titanium Carbide (MXene). *ACS Appl Mater Interfaces* **2017,** *9* (42), 37184-37190.
13. Mirzaei, A.; Kim, J.-H.; Kim, H. W.; Kim, S. S., How shell thickness can affect the gas sensing properties of nanostructured materials: Survey of literature. *Sensors and Actuators B: Chemical* **2018,** *258*, 270-294.
14. Kannan, V., Adsorption studies on small toxic gases using silicane nanosheet as a chemi-resistive sensor – DFT method. *Computational and Theoretical Chemistry* **2020,** *1191*.
15. Fæhn, T.; Hagem, C.; Lindholt, L.; Mæland, S.; Rosendahl, K. E. J. T. E. J., Climate policies in a fossil fuel producing country–demand versus supply side policies. *The Energy Journal* **2017,** *38* (1).

16. Barea, E.; Montoro, C.; Navarro, J. A. J. C. S. R., Toxic gas removal–metal–organic frameworks for the capture and degradation of toxic gases and vapours. *Chemical Society Reviews* **2014,** *43* (16), 5419-5430.

17. Rahman, F. A.; Aziz, M. M. A.; Saidur, R.; Bakar, W. A. W. A.; Hainin, M.; Putrajaya, R.; Hassan, N. A. J. R.; Reviews, S. E., Pollution to solution: Capture and sequestration of carbon dioxide (CO2) and its utilization as a renewable energy source for a sustainable future. *Renewable and Sustainable Energy Reviews* **2017,** *71*, 112-126.

18. Grennfelt, P.; Engleryd, A.; Forsius, M.; Hov, O.; Rodhe, H.; Cowling, E., Acid rain and air pollution: 50 years of progress in environmental science and policy. *Ambio* **2020,** *49* (4), 849-864.

19. Heinemann, S. H.; Hoshi, T.; Westerhausen, M.; Schiller, A. J. C. C., Carbon monoxide–physiology, detection and controlled release. *Chemical Communications* **2014,** *50* (28), 3644-3660.

20. Mirzaei, A.; Leonardi, S. G.; Neri, G., Detection of hazardous volatile organic compounds (VOCs) by metal oxide nanostructures-based gas sensors: A review. *Ceramics International* **2016,** *42* (14), 15119-15141.

21. Neubert, S.; Roddelkopf, T.; Al-Okby, M. F. R.; Junginger, S.; Thurow, K. J. S., Flexible IoT Gas Sensor Node for Automated Life Science Environments Using Stationary and Mobile Robots. *Sensors* **2021,** *21* (21), 7347.

22. Bogue, R. J. S. R., Energy harvesting and wireless sensors: a review of recent developments. *Sensor Review* **2009,** *29*, 194-199.

23. Kang, X.; Yip, S.; Meng, Y.; Wang, W.; Li, D.; Liu, C.; Ho, J. C., High-performance electrically transduced hazardous gas sensors based on low-dimensional nanomaterials. *Nanoscale Advances* **2021,** *3* (22), 6254-6270.

24. Nazemi, H.; Joseph, A.; Park, J.; Emadi, A. J. S., Advanced micro-and nano-gas sensor technology: A review. *Sensors* **2019,** *19* (6), 1285.

25. Sanyal, G.; Vaidyanathan, A.; Rout, C. S.; Chakraborty, B., Recent developments in two-dimensional layered tungsten dichalcogenides based materials for gas sensing applications. *Materials Today Communications* **2021,** *28*.

26. Tricoli, A.; Righettoni, M.; Teleki, A. J. A. C. I. E., Semiconductor gas sensors: dry synthesis and application. *Angewandte Chemie International Edition* **2010,** *49* (42), 7632-7659.

27. Yuan, W.; Shi, G. J. J. o. M. C. A., Graphene-based gas sensors. *Journal of Materials Chemistry A* **2013,** *1* (35), 10078-10091.

28. Chen, X.; Chen, X.; Han, Y.; Su, C.; Zeng, M.; Hu, N.; Su, Y.; Zhou, Z.; Wei, H.; Yang, Z. J. N., Two-dimensional MoSe2 nanosheets via liquid-phase exfoliation for high-performance room temperature NO2 gas sensors. *Nanotechnology* **2019,** *30* (44), 445503.

29. Yang, S.; Jiang, C.; Wei, S.-h., Gas sensing in 2D materials. *Applied Physics Reviews* **2017,** *4* (2).

30. Yang, T.; Liu, Y.; Wang, H.; Duo, Y.; Zhang, B.; Ge, Y.; Zhang, H.; Chen,

W. J. J. o. M. C. C., Recent advances in 0D nanostructure-functionalized low-dimensional nanomaterials for chemiresistive gas sensors. *Journal of Materials Chemistry C* **2020,** *8* (22), 7272-7299.

31. Dong, C.; Zhao, R.; Yao, L.; Ran, Y.; Zhang, X.; Wang, Y. J. J. o. A.; Compounds, A review on WO3 based gas sensors: Morphology control and enhanced sensing properties. *Journal of Alloys and Compounds* **2020,** *820*, 153194.

32. Galstyan, V.; Moumen, A.; Kumarage, G. W.; Comini, E. J. S.; Chemical, A. B., Progress towards chemical gas sensors: Nanowires and 2D semiconductors. *Sensors and Actuators B: Chemical* **2022**, 131466.

33. Tonezzer, M.; Dang, T. T. L.; Bazzanella, N.; Nguyen, V. H.; Iannotta, S., Comparative gas-sensing performance of 1D and 2D ZnO nanostructures. *Sensors and Actuators B: Chemical* **2015,** *220*, 1152-1160.

34. Qin, R.; Shan, G.; Hu, M.; Huang, W. J. M. T. P., Two-dimensional transition metal carbides and/or nitrides (MXenes) and their applications in sensors. *Materials Today Physics* **2021,** *21*, 100527.

35. Choi, S.-J.; Kim, I.-D. J. E. M. L., Recent developments in 2D nanomaterials for chemiresistive-type gas sensors. *Electronic Materials Letters* **2018,** *14* (3), 221-260.

36. Larsen, P. M.; Pandey, M.; Strange, M.; Jacobsen, K. W. J. P. R. M., Definition of a scoring parameter to identify low-dimensional materials components. *Physical Review Materials* **2019,** *3* (3), 034003.

37. Wang, F.; Wang, Z.; Shifa, T. A.; Wen, Y.; Wang, F.; Zhan, X.; Wang, Q.; Xu, K.; Huang, Y.; Yin, L. J. A. F. M., Two-dimensional non-layered materials: synthesis, properties and applications. *Advanced Functional Materials* **2017,** *27* (19), 1603254.

38. Cai, Z.; Liu, B.; Zou, X.; Cheng, H.-M. J. C. r., Chemical vapor deposition growth and applications of two-dimensional materials and their heterostructures. *Chemical reviews* **2018,** *118* (13), 6091-6133.

39. Xu, X.; Hu, D.; Yan, L.; Fang, S.; Shen, C.; Loo, Y. L.; Lin, Y.; Haines, C. S.; Li, N.; Zakhidov, A. A. J. A. M., Polar-electrode-bridged electroluminescent displays: 2D sensors remotely communicating optically. *Advanced Materials* **2017,** *29* (41), 1703552.

40. Zhang, D.; Li, L.; Deng, J.; Gou, Y.; Fang, J.; Cui, H.; Zhao, Y.; Shang, K. J. C., Application of 2D Materials to Potassium - Ion Hybrid Capacitors. *ChemSusChem* **2021,** *14* (9), 1974-1986.

41. Schedin, F.; Geim, A. K.; Morozov, S. V.; Hill, E. W.; Blake, P.; Katsnelson, M. I.; Novoselov, K. S. J. N. m., Detection of individual gas molecules adsorbed on graphene. *Nature materials* **2007,** *6* (9), 652-655.

42. Mukhopadhyay, P.; Gupta, R. K., *Graphite, graphene, and their polymer nanocomposites*. CRC press: 2012.

43. Alwarappan, S.; Kumar, A., *Graphene-based materials: science and technology*. CRC Press: 2013.

44. Novoselov, K. S.; Geim, A. K.; Morozov, S. V.; Jiang, D.-e.; Zhang, Y.; Dubonos, S. V.; Grigorieva, I. V.; Firsov, A. A. J. s., Electric field effect in atomically thin carbon films. *science* **2004,** *306* (5696), 666-669.

45. Xu, Q.; Dai, Y.; Peng, Y.; Hong, L.; Yang, N.; Wang, Z. J. S., Recent Development of Multifunctional Sensors Based on Low-Dimensional Materials. *Sensors (Basel)* **2021,** *21* (22), 7727.

46. Basu, S.; Bhattacharyya, P. J. S.; Chemical, A. B., Recent developments on graphene and graphene oxide based solid state gas sensors. *Sensors and Actuators B: Chemical* **2012,** *173*, 1-21.

47. Chen, N.; Li, X.; Wang, X.; Yu, J.; Wang, J.; Tang, Z.; Akbar, S. J. S.; Chemical, A. B., Enhanced room temperature sensing of Co3O4-intercalated reduced graphene oxide based gas sensors. *Sensors and Actuators B: Chemical* **2013,** *188*, 902-908.

48. Walia, G. K.; Randhawa, D. K. K.; Malhi, K. S., Rise of silicene and its applications in gas sensing. *J Mol Model* **2021,** *27* (10), 277.

49. Gupta, S. K.; Singh, D.; Rajput, K.; Sonvane, Y., Germanene: a new electronic gas sensing material. *RSC Advances* **2016,** *6* (104), 102264-102271.

50. Zhang, A.; Yang, H.; Liu, Q.; Li, W.; Wang, Y. J. S. M., DFT insights into the adsorption properties of toxic gas molecules on pure and transition metal embedded stanene monolayers: Towards gas sensor devices. *Synthetic Metals* **2020,** *266*, 116441.

51. Tareen, A. K.; Khan, K.; Rehman, S.; Iqbal, M.; Yu, J.; Zhou, Z.; Yin, J.; Zhang, H. J. P. i. S. S. C., Recent development in emerging phosphorene based novel materials: Progress, challenges, prospects and their fascinating sensing applications. *Progress in Solid State Chemistry* **2022,** *65*, 100336.

52. Zhou, R.; Xu, N.; Guo, R.; Ling, G.; Zhang, P. J. J. o. P. D. A. P., Preparation of arsenene and its applications in sensors. *Journal of Physics D: Applied Physics* **2021,** *55* (16), 163002.

53. Meng, R.-S.; Cai, M.; Jiang, J.-K.; Liang, Q.-H.; Sun, X.; Yang, Q.; Tan, C.-J.; Chen, X.-P. J. I. E. D. L., First principles investigation of small molecules adsorption on antimonene. *IEEE Electron Device Letters* **2016,** *38* (1), 134-137.

54. Hou, C.; Tai, G.; Liu, Y.; Liu, X. J. N. R., Borophene gas sensor. *Nano Research* **2022,** *15* (3), 2537-2544.

55. Shi, J.; Quan, W.; Chen, X.; Chen, X.; Zhang, Y.; Lv, W.; Yang, J.; Zeng, M.; Wei, H.; Hu, N.; Su, Y.; Zhou, Z.; Yang, Z., Noble metal (Ag, Au, Pd and Pt) doped TaS2 monolayer for gas sensing: a first-principles investigation. *Phys Chem Chem Phys* **2021,** *23* (34), 18359-18368.

56. Li, B. L.; Wang, J.; Zou, H. L.; Garaj, S.; Lim, C. T.; Xie, J.; Li, N. B.; Leong, D. T. J. A. F. M., Low - dimensional transition metal dichalcogenide nanostructures based sensors. *Advanced Functional Materials* **2016,** *26* (39), 7034-7056.

57. Kumar, S.; Pavelyev, V.; Mishra, P.; Tripathi, N.; Sharma, P.; Calle, F., A

review on 2D transition metal di-chalcogenides and metal oxide nanostructures based NO2 gas sensors. *Materials Science in Semiconductor Processing* **2020,** *107*.

58. Barsoum, M.; Golczewski, J.; Seifert, H.; Aldinger, Fabrication and electrical and thermal properties of Ti2InC, Hf2InC and (Ti, Hf) 2InC. *Journal of alloys compounds* **2002,** *340* (1-2), 173-179.

59. Ding, L.; Wei, Y.; Wang, Y.; Chen, H.; Caro, J.; Wang, H., A two - dimensional lamellar membrane: MXene nanosheet stacks. *Angewandte Chemie International Edition* **2017,** *56* (7), 1825-1829.

60. Lee, E.; Kim, D.-J., Recent exploration of two-dimensional MXenes for gas sensing: From a theoretical to an experimental view. *Journal of The Electrochemical Society* **2019,** *167* (3), 037515.

61. Tang, X.; Du, A.; Kou, L., Gas sensing and capturing based on two - dimensional layered materials: Overview from theoretical perspective. *WIREs Computational Molecular Science* **2018,** *8* (4).

62. Zhang, W.; Zhang, Y.; Qiu, J.; Zhao, Z.; Liu, N. J. I., Topological structures of transition metal dichalcogenides: A review on fabrication, effects, applications, and potential. *InfoMat* **2021,** *3* (2), 133-154.

63. Kumbhakar, P.; Gowda, C. C.; Mahapatra, P. L.; Mukherjee, M.; Malviya, K. D.; Chaker, M.; Chandra, A.; Lahiri, B.; Ajayan, P.; Jariwala, D. J. M. T., Emerging 2D metal oxides and their applications. *Materials Today* **2021,** *45*, 142-168.

64. Fan, Y.; Li, L.; Zhang, Y.; Zhang, X.; Geng, D.; Hu, W. J. A. F. M., Recent advances in growth of transition metal carbides and nitrides (MXenes) crystals. *Advanced Functional Materials* **2022,** *32* (16), 2111357.

65. Mirabelli, G.; McGeough, C.; Schmidt, M.; McCarthy, E. K.; Monaghan, S.; Povey, I. M.; McCarthy, M.; Gity, F.; Nagle, R.; Hughes, G.; Cafolla, A.; Hurley, P. K.; Duffy, R., Air sensitivity of MoS2, MoSe2, MoTe2, HfS2, and HfSe2. *Journal of Applied Physics* **2016,** *120* (12).

66. Shi, Y.; Li, H.; Li, L.-J. J. C. S. R., Recent advances in controlled synthesis of two-dimensional transition metal dichalcogenides via vapour deposition techniques. *Chemical Society Reviews* **2015,** *44* (9), 2744-2756.

67. Mishra, N.; Pandey, B. P.; Kumar, B.; Kumar, S., Enhanced electronic and magnetic properties of N 2 O gas adsorbed Mn-doped MoSe2 monolayer. *IEEE Transactions on Electron Devices* **2021,** *69* (4), 1634-1641.

68. Li, B. L.; Wang, J.; Zou, H. L.; Garaj, S.; Lim, C. T.; Xie, J.; Li, N. B.; Leong, D. T., Low-Dimensional Transition Metal Dichalcogenide Nanostructures Based Sensors. *Advanced Functional Materials* **2016,** *26* (39), 7034-7056.

69. Jiang, T.; He, Q.; Bi, M.; Chen, X.; Sun, H.; Tao, L., First-principles calculations of adsorption sensitivity of Au-doped MoS2 gas sensor to main characteristic gases in oil. *Journal of Materials Science* **2021,** *56* (24), 13673-13683.

70. Shokri, A.; Salami, N. J. S.; Chemical, A. B., Gas sensor based on MoS2 monolayer. *Sensors and Actuators B: Chemical* **2016,** *236*, 378-385.

71. Cho, B.; Kim, A. R.; Park, Y.; Yoon, J.; Lee, Y.-J.; Lee, S.; Yoo, T. J.;

Kang, C. G.; Lee, B. H.; Ko, H. C., Bifunctional sensing characteristics of chemical vapor deposition synthesized atomic-layered MoS2. *ACS applied materials & interfaces* **2015,** *7* (4), 2952-2959.

72. Zhou, C.; Yang, W.; Zhu, H. J. T. J. o. c. p., Mechanism of charge transfer and its impacts on Fermi-level pinning for gas molecules adsorbed on monolayer WS2. *The Journal of chemical physics* **2015,** *142* (21), 214704.

73. Late, D. J.; Huang, Y. K.; Liu, B.; Acharya, J.; Shirodkar, S. N.; Luo, J.; Yan, A.; Charles, D.; Waghmare, U. V.; Dravid, V. P.; Rao, C. N., Sensing behavior of atomically thin-layered MoS2 transistors. *ACS Nano* **2013,** *7* (6), 4879-91.

74. Rahman, M.; Davey, K.; Qiao, S. Z., Advent of 2D Rhenium Disulfide (ReS2): Fundamentals to Applications. *Advanced Functional Materials* **2017,** *27* (10).

75. Obodo, K. O.; Ouma, C. N. M.; Obodo, J. T.; Braun, M., Influence of transition metal doping on the electronic and optical properties of ReS2 and ReSe2 monolayers. *Phys Chem Chem Phys* **2017,** *19* (29), 19050-19057.

76. Murray, H. H.; Kelty, S. P.; Chianelli, R. R.; Day, C. S., Structure of Rhenium Disulfide. *Inorganic Chemistry* **1994,** *33* (19), 4418-4420.

77. Pan, J.; Zhou, X.; Zhong, J.; Hu, J. J. P. L. A., Induction of an atomically thin ferromagnetic semiconductor in 1T′ phase ReS2 by doping with transition metals. *Physics Letters A* **2019,** *383* (31), 125883.

78. Lamfers, H.-J.; Meetsma, A.; Wiegers, G.; De Boer, J., The crystal structure of some rhenium and technetium dichalcogenides. *Journal of alloys compounds* **1996,** *241* (1-2), 34-39.

79. Liu, E.; Fu, Y.; Wang, Y.; Feng, Y.; Liu, H.; Wan, X.; Zhou, W.; Wang, B.; Shao, L.; Ho, C. H.; Huang, Y. S.; Cao, Z.; Wang, L.; Li, A.; Zeng, J.; Song, F.; Wang, X.; Shi, Y.; Yuan, H.; Hwang, H. Y.; Cui, Y.; Miao, F.; Xing, D., Integrated digital inverters based on two-dimensional anisotropic ReS2 field-effect transistors. *Nat Commun* **2015,** *6*, 6991.

80. Li, J.; Chen, X.; Yang, Z.; Liu, X.; Zhang, X. J. J. o. M. C. C., Highly anisotropic gas sensing of atom-thin borophene: a first-principles study. *Journal of Materials Chemistry C* **2021,** *9* (3), 1069-1076.

81. Yang, S.; Tongay, S.; Li, Y.; Yue, Q.; Xia, J. B.; Li, S. S.; Li, J.; Wei, S. H., Layer-dependent electrical and optoelectronic responses of ReSe2 nanosheet transistors. *Nanoscale* **2014,** *6* (13), 7226-31.

82. Ho, C. H.; Huang, Y. S.; Tiong, K. K., In-plane anisotropy of the optical and electrical properties of ReS2 and ReSe2 layered crystals. *Journal of Alloys and Compounds* **2001,** *317-318*, 222-226.

83. Xu, K.; Deng, H. X.; Wang, Z.; Huang, Y.; Wang, F.; Li, S. S.; Luo, J. W.; He, J., Sulfur vacancy activated field effect transistors based on ReS2 nanosheets. *Nanoscale* **2015,** *7* (38), 15757-62.

84. Hafeez, M.; Gan, L.; Saleem Bhatti, A.; Zhai, T., Rhenium dichalcogenides (ReX2, X = S or Se): an emerging class of TMDs family. *Materials Chemistry Frontiers* **2017,** *1* (10), 1917-1932.

85. Martin-Garcia, B.; Spirito, D.; Bellani, S.; Prato, M.; Romano, V.; Polovitsyn, A.; Brescia, R.; Oropesa-Nunez, R.; Najafi, L.; Ansaldo, A.; D'Angelo, G.; Pellegrini, V.; Krahne, R.; Moreels, I.; Bonaccorso, F., Extending the Colloidal Transition Metal Dichalcogenide Library to ReS2 Nanosheets for Application in Gas Sensing and Electrocatalysis. *Small* **2019,** *15* (52), e1904670.

86. Jariwala, B.; Voiry, D.; Jindal, A.; Chalke, B. A.; Bapat, R. D.; Thamizhavel, A.; Chhowalla, M.; Deshmukh, M. M.; Bhattacharya, A., Synthesis and Characterization of ReS2 and ReSe2 Layered Chalcogenide Single Crystals. *Chemistry of Materials* **2016,** *28*, 3352-3359.

87. Myronov, M., Molecular Beam Epitaxy of High Mobility Silicon, Silicon Germanium and Germanium Quantum Well Heterostructures. In *Molecular Beam Epitaxy*, Elsevier: 2018; pp 37-54.

88. Zulkefli, A.; Mukherjee, B.; Sahara, R.; Hayakawa, R.; Iwasaki, T.; Wakayama, Y.; Nakaharai, S., Enhanced Selectivity in Volatile Organic Compound Gas Sensors Based on ReS2-FETs under Light-Assisted and Gate-Bias Tunable Operation. *ACS Appl Mater Interfaces* **2021,** *13* (36), 43030-43038.

89. Zhou, Q.; Luo, S.; Xue, W.; Liao, N. J. A. S. S., Highly selective nitrogen dioxide gas sensing of ReS2 nanosheets: A first-principles study. *Applied Surface Science* **2022**, 155388.

90. Yang, G.; Lee, C.; Kim, J.; Ren, F.; Pearton, S. J., Flexible graphene-based chemical sensors on paper substrates. *Phys Chem Chem Phys* **2013,** *15* (6), 1798-801.

91. Yang, A.; Gao, J.; Li, B.; Tan, J.; Xiang, Y.; Gupta, T.; Li, L.; Suresh, S.; Idrobo, J. C.; Lu, T.-M.; Rong, M.; Koratkar, N., Humidity sensing using vertically oriented arrays of ReS2 nanosheets deposited on an interdigitated gold electrode. *2D Materials* **2016,** *3* (4).

92. Huo, N.; Yang, S.; Wei, Z.; Li, S.-S.; Xia, J.-B.; Li, J., Photoresponsive and Gas Sensing Field-Effect Transistors based on Multilayer WS2 Nanoflakes. *Scientific Reports* **2014,** *4* (1), 5209.

93. Chen, P.; Wang, J.; Lu, Y.; Zhang, S.; Liu, X.; Hou, W.; Wang, Z.; Wang, L., The fabrication of ReS2 flowers at controlled locations by chemical vapor deposition. *Physica E: Low-dimensional Systems and Nanostructures* **2017,** *89*, 115-118.

94. Zeng, Y.; Lin, S.; Gu, D.; Li, X., Two-Dimensional Nanomaterials for Gas Sensing Applications: The Role of Theoretical Calculations. *Nanomaterials (Basel)* **2018,** *8* (10).

95. Sholl, D. S.; Steckel, J. A., *Density functional theory: a practical introduction*. John Wiley & Sons: 2011.

96. Boboriko, N. E.; Dzichenka, Y. U., Molecular dynamics simulation as a tool for prediction of the properties of TiO2 and TiO2: MoO3 based chemical gas sensors. *Journal of Alloys Compounds* **2021,** *855*, 157490.

97. Hirose, K., *First-principles Calculations in Real-space Formalism: Electronic Configurations and Transport Properties of Nanostructures*. Imperial

College Press: 2005.

98. Dolg, F. M., *Progress in Physical Chemistry Volume 3*. De Gruyter.: 2011.

99. Pozhar, L., *Virtual Synthesis of Nanosystems by Design: From First Principles to Applications*. Elsevier: 2015.

100. Espanol, P.; Lowen, H., Derivation of dynamical density functional theory using the projection operator technique. *J Chem Phys* **2009,** *131* (24), 244101.

101. Kestyn, J.; Polizzi, E., From Fundamental First-Principle Calculations to Nanoengineering Applications: A Review of the NESSIE Project. *IEEE Nanotechnology Magazine* **2020,** *14* (6), 52-C3.

102. Parr, R. G., Density functional theory of atoms and molecules. In *Horizons of quantum chemistry*, Springer: 1980; pp 5-15.

103. McDouall, J. J., *Computational quantum chemistry: molecular structure and properties in silico*. Royal Society of Chemistry: 2013.

104. Reimers, J. R., *Computational methods for large systems: electronic structure approaches for biotechnology and nanotechnology*. John Wiley & Sons: 2011.

105. Kraisler, E., Asymptotic Behavior of the Exchange‐Correlation Energy Density and the Kohn‐Sham Potential in Density Functional Theory: Exact Results and Strategy for Approximations. *Israel Journal of Chemistry* **2020,** *60* (8-9), 805-822.

106. Cramer, C. J.; Bickelhaupt, F., Essentials of computational chemistry. *ANGEWANDTE CHEMIE-INTERNATIONAL EDITION IN ENGLISH-* **2003,** *42* (4), 381-381.

107. Simon, L.; Goodman, J. M., How reliable are DFT transition structures? Comparison of GGA, hybrid-meta-GGA and meta-GGA functionals. *Org Biomol Chem* **2011,** *9* (3), 689-700.

108. Chen, D.-L.; Al-Saidi, W. A.; Karl Johnson, J., The role of van der Waals interactions in the adsorption of noble gases on metal surfaces. *Journal of physics. Condensed matter* **2012,** *24* (42), 424211-424211.

109. Mehta, S.; Price, G. D.; Alfe, D., Ab initio thermodynamics and phase diagram of solid magnesium: a comparison of the LDA and GGA. *J Chem Phys* **2006,** *125* (19), 194507.

110. Perdew, J. P.; Burke, K.; Ernzerhof, M., Generalized Gradient Approximation Made Simple [Phys. Rev. Lett. 77, 3865 (1996)]. *Physical Review Letters* **1997,** *78* (7), 1396-1396.

111. Perdew, J. P.; Chevary, J. A.; Vosko, S. H.; Jackson, K. A.; Pederson, M. R.; Singh, D. J.; Fiolhais, C., Atoms, molecules, solids, and surfaces: Applications of the generalized gradient approximation for exchange and correlation. *Physical Review B* **1992,** *46* (11), 6671-6687.

112. Zhang, Y.; Yang, W., Comment on ``Generalized Gradient Approximation Made Simple". *Physical Review Letters* **1998,** *80* (4), 890-890.

113. Hammer, B.; Hansen, L. B.; Norskov, J. K., Improved adsorption energetics within density-functional theory using revised Perdew-Burke-Ernzerhof functionals.

Physical review. B **1999,** *59* (11), 7413-7421.

114. Grimme, S., Accurate description of van der Waals complexes by density functional theory including empirical corrections. *J Comput Chem* **2004,** *25* (12), 1463-73.

115. Caldeweyher, E.; Bannwarth, C.; Grimme, S., Extension of the D3 dispersion coefficient model. *J Chem Phys* **2017,** *147* (3), 034112.

116. Mulliken, R. S., Electronic Population Analysis on LCAO–MO Molecular Wave Functions. I. *The Journal of Chemical Physics* **1955,** *23* (10), 1833-1840.

117. Becke, A., *The quantum theory of atoms in molecules: from solid state to DNA and drug design*. John Wiley & Sons: 2007.

118. Hirshfeld, F. L., Bonded-atom fragments for describing molecular charge densities. *Theoretica chimica acta* **1977,** *44* (2), 129-138.

119. Wiberg, K. B.; Rablen, P. R., Atomic charges. *The Journal of Organic Chemistry* **2018,** *83* (24), 15463-15469.

120. Marenich, A. V.; Jerome, S. V.; Cramer, C. J.; Truhlar, D. G., Charge model 5: An extension of Hirshfeld population analysis for the accurate description of molecular interactions in gaseous and condensed phases. *Journal of chemical theory computation* **2012,** *8* (2), 527-541.

121. Vilseck, J. Z.; Tirado-Rives, J.; Jorgensen, W. L., Evaluation of CM5 charges for condensed-phase modeling. *Journal of chemical theory computation* **2014,** *10* (7), 2802-2812.

122. Fonseca Guerra, C.; Handgraaf, J. W.; Baerends, E. J.; Bickelhaupt, F. M., Voronoi deformation density (VDD) charges: Assessment of the Mulliken, Bader, Hirshfeld, Weinhold, and VDD methods for charge analysis. *J Comput Chem* **2004,** *25* (2), 189-210.

123. Maslen, E.; Spackman, M., Atomic charges and electron density partitioning. *Australian journal of physics* **1985,** *38* (3), 273-288.

124. Savin, A.; Nesper, R.; Wengert, S.; Fässler, T. F., ELF: The Electron Localization Function. *Angewandte Chemie International Edition in English* **1997,** *36* (17), 1808-1832.

125. Becke, A. D.; Edgecombe, K. E., A simple measure of electron localization in atomic and molecular systems. **1990,** *92* (9), 5397-5403.

126. Wagner, F. R., Electron localizability: chemical bonding analysis in direct and momentum space. *Max-Planck-Institut fÃ¼r Chemische Physik fester Stoffe http://www2. cpfs. mpg. de/ELF/index. php* **2002**.

127. Larino, R. C., Introduction to Density Functional Theory Calculations.

128. Cortés-Arriagada, D.; Villegas-Escobar, N., A DFT analysis of the adsorption of nitrogen oxides on Fe-doped graphene, and the electric field induced desorption. *Applied Surface Science* **2017,** *420*, 446-455.

129. Niu, F.; Cai, M.; Pang, J.; Li, X.; Zhang, G.; Yang, D., A first-principles study: Adsorption of small gas molecules on GeP3 monolayer. *Surface Science* **2019,** *684*, 37-43.

130. Te Velde, G.; Baerends, E., Precise density-functional method for periodic structures. *Physical Review B* **1991,** *44* (15), 7888.

131. Wiesenekker, G.; Baerends, E., Quadratic integration over the three-dimensional Brillouin zone. *Journal of Physics: Condensed Matter* **1991,** *3* (35), 6721.

132. Franchini, M.; Philipsen, P. H. T.; Visscher, L., The Becke fuzzy cells integration scheme in the Amsterdam Density Functional program suite. *Journal of computational chemistry* **2013,** *34* (21), 1819-1827.

133. Franchini, M.; Philipsen, P. H. T.; van Lenthe, E.; Visscher, L., Accurate coulomb potentials for periodic and molecular systems through density fitting. *Journal of chemical theory computation* **2014,** *10* (5), 1994-2004.

134. P.H.T. Philipsen, G. t. V., E.J. Baerends, J.A. Berger, P.L. de Boeij, M. Franchini, J.A. Groeneveld, E.S. Kadantsev, R. Klooster, F. Kootstra, P. Romaniello, M. Raupach, D.G. Skachkov, J.G. Snijders, C.J.O. Verzijl, J.A. Celis Gil, J. M. Thijssen, G. Wiesenekker, T. Ziegler.,BAND 2021.1, SCM, Theoretical Chemistry, Vrije Universiteit, Amsterdam, The Netherlands, http://www.scm.com.

135. Grimme, S.; Bannwarth, C.; Shushkov, P., A Robust and Accurate Tight-Binding Quantum Chemical Method for Structures, Vibrational Frequencies, and Noncovalent Interactions of Large Molecular Systems Parametrized for All spd-Block Elements (Z = 1–86). *Journal of chemical theory and computation* **2017,** *13* (5), 1989-2009.

136. Persson, K., Materials Data on ReS2 (SG:2) by Materials Project. 2014.

137. Zong, J.-Q.; Zhang, S.-F.; Ji, W.-X.; Zhang, C.-W.; Li, P.; Wang, P.-J., Electric structure and optical properties of ReS2 nanomaterials. *Superlattices and Microstructures* **2018,** *122*, 262-267.

138. Hu, Z.; Zhang, S.; Zhang, Y. N.; Wang, D.; Zeng, H.; Liu, L. M., Modulating the phase transition between metallic and semiconducting single-layer MoS2 and WS2 through size effects. *Phys Chem Chem Phys* **2015,** *17* (2), 1099-105.

139. Liu, H.; Xu, B.; Liu, J.-M.; Yin, J.; Miao, F.; Duan, C.-G.; Wan, X., Highly efficient and ultrastable visible-light photocatalytic water splitting over ReS2. *Physical Chemistry Chemical Physics* **2016,** *18* (21), 14222-14227.

140. CO2 emissions (kt). https://data.worldbank.org/indicator/EN.ATM.CO2E.KT.

141. Prockop, L. D.; Chichkova, R. I., Carbon monoxide intoxication: An updated review. *Journal of the neurological sciences* **2007,** *262* (1), 122-130.

142. Guo, X.; Song, Q.; Wang, H.; Li, N.; Su, W.; Liang, M.; Sun, C.; Ding, X.; Liang, Q.; Sun, Y., Systematic review and meta-analysis of studies between short-term exposure to ambient carbon monoxide and non-accidental, cardiovascular, and respiratory mortality in China. *Environ Sci Pollut Res Int* **2022,** *29* (24), 35707-35722.

143. Aykanat, A.; Meng, Z.; Stolz, R. M.; Morrell, C. T.; Mirica, K. A., Bimetallic Two‐Dimensional Metal–Organic Frameworks for the Chemiresistive Detection of Carbon Monoxide. *Angewandte Chemie (International ed.)* **2022,** *61* (6), e202113665-n/a.

144. Sun, R.; Pu, L.; Yu, H.; Dai, M.; Li, Y., Modeling the diffusion of

flammable hydrogen cloud under different liquid hydrogen leakage conditions in a hydrogen refueling station. *International Journal of Hydrogen Energy* **2022,** *47* (61), 25849-25863.

145. Le, H.-J.; Van Dao, D.; Yu, Y.-T., Superfast and efficient hydrogen gas sensor using PdAualloy@ZnO core-shell nanoparticles. *Journal of materials chemistry. A, Materials for energy and sustainability* **2020,** *8* (26), 12968-12974.

146. Zhao, Z.; Yong, Y.; Gao, R.; Hu, S.; Zhou, Q.; Kuang, Y. J. V., Enhancement of nitride-gas sensing performance of SiC7 monolayer induced by external electric field. *Vacuum* **2021,** *191*, 110393.

147. Shen, Y.; Jiang, F.; Feng, S.; Zheng, Y.; Cai, Z.; Lyu, X., Impact of weather and emission changes on NO2 concentrations in China during 2014–2019. *Environmental pollution (1987)* **2021,** *269*, 116163.

148. Faustini, A.; Rapp, R.; Forastiere, F., Nitrogen dioxide and mortality: Review and meta-analysis of long-term studies. *The European respiratory journal* **2014,** *44* (3), 744-753.

149. Alderton, W. K.; Cooper, C. E.; Knowles, R. G. J. B. j., Nitric oxide synthases: structure, function and inhibition. *Biochemical journal* **2001,** *357* (3), 593-615.

150. Haefliger, I.; Flammer, J.; Lüscher, T. J. I. o.; science, v., Nitric oxide and endothelin-1 are important regulators of human ophthalmic artery. *Investigative ophthalmology & visual science* **1992,** *33* (7), 2340-2343.

151. Malik, M. A. J. P. C.; Processing, P., Nitric oxide production by high voltage electrical discharges for medical uses: a review. *Plasma Chemistry and Plasma Processing* **2016,** *36* (3), 737-766.

152. Li, C.; Song, B.-Y.; Lv, M.-S.; Chen, G.-L.; Zhang, X.-F.; Deng, Z.-P.; Xu, Y.-M.; Huo, L.-H.; Gao, S., Highly sensitive and selective nitric oxide sensor based on biomorphic ZnO microtubes with dual-defects assistance at low temperature. *Chemical engineering journal (Lausanne, Switzerland : 1996)* **2022,** *446*, 136846.

153. McCleverty, J., Chemistry of nitric oxide relevant to biology. *Chemical reviews* **2004,** *104* (2), 403-418.

154. Yue, Q.; Shao, Z.; Chang, S.; Li, J., Adsorption of gas molecules on monolayer MoS2 and effect of applied electric field. *Nanoscale research letters* **2013,** *8* (1), 1-7.

155. Jiao, Y.; Ma, F.; Zhang, X.; Heine, T., A perfect match between borophene and aluminium in the AlB 3 heterostructure with covalent Al–B bonds, multiple Dirac points and a high Fermi velocity. *Chemical science* **2022,** *13* (4), 1016-1022.

156. Lepetit, C.; Fau, P.; Fajerwerg, K.; Kahn, M. L.; Silvi, B., Topological analysis of the metal-metal bond: A tutorial review. *Coordination Chemistry Reviews* **2017,** *345*, 150-181.

157. Rajkumar, K.; Kumar, R. T. R., Chapter 6 - Gas Sensors Based on Two-Dimensional Materials and Its Mechanisms. In *Fundamentals and Sensing Applications of 2D Materials*, Hywel, M.; Rout, C. S.; Late, D. J., Eds. Woodhead

Publishing: 2019; pp 205-258.